Landscape and regulation of mRNA translation in the early *C. elegans* embryo

Yash Shukla[1], Vighnesh Ghatpande[1], Cindy F. Hu[1], Daniel J. Dickinson[1] and Can Cenik[1]**

[1]Department of Molecular Biosciences, The University of Texas at Austin, Austin, TX 78712, USA

*Correspondence: daniel.dickinson@austin.utexas.edu, ccenik@austin.utexas.edu

Summary

Animal embryos rely on regulated translation of maternally deposited mRNAs to drive early development. Using low-input ribosome profiling combined with RNA sequencing on precisely staged embryos, we measured mRNA translation during the first four cell cycles of *C. elegans* development. We uncovered stage-specific patterns of developmentally coordinated translational regulation. We confirmed that mRNA localization correlates with translational efficiency, though initial translational repression in germline precursors occurs before P-granule association. Our analysis suggests that the RNA-binding protein OMA-1 represses the translation of its target mRNAs in a stage-specific manner, while indirectly promoting the translational efficiency of other transcripts. These findings illuminate how post-transcriptional mechanisms shape the embryonic proteome to direct cell differentiation, with implications for understanding similar regulation across species where maternal factors guide early development.

Keywords

mRNA translation, translational regulation, *C. elegans*, embryogenesis, ribosome profiling, Ribo-ITP, OMA-1, P-granules, maternal transcripts, post-transcriptional control, cell fate determination

1. Introduction

During animal development, a single-cell zygote undergoes cleavage to produce founder blastomeres that subsequently form specialized organs and tissues. The early embryo must precisely regulate protein expression both spatially and temporally, despite being transcriptionally quiescent to varying degrees[1]. To overcome this challenge, embryos rely on post-transcriptional regulation of maternally deposited proteins and mRNAs[2]. Post-transcriptional regulation is particularly critical prior to the maternal-to-zygotic transition, when the embryo begins to rely on newly generated transcripts from its own genome[3]. However,

post-transcriptional regulation continues to play important roles beyond the maternal-to-zygotic transition in many species, as maternal mRNAs influence development even after zygotic genome activation[4,5] .

In *C. elegans*, the embryonic cell lineage is invariant, with cell fates becoming irreversibly determined beginning from the first cleavage[6]. Notably, this irreversible cell differentiation occurs in the absence of new mRNA synthesis[7,8]. This early specification raises the intriguing question of how cell fates are determined before the activation of the zygotic genome. In most other organisms, cell fate determination relies on both transcriptional and translational regulation[2] ; thus, *C. elegans* offers a unique opportunity to study translational control in isolation during early development. Recent work has further demonstrated that maternal ribosomes alone are sufficient for embryonic development in *C. elegans*[9], suggesting that the translation machinery established in the oocyte is capable of sustaining early developmental processes.

Although single-cell RNA-seq studies have revealed maternal transcript abundance in individual cells within early *C. elegans* embryos (1-16 cells)[8,10–12], our understanding of spatiotemporal control of mRNA translation remains limited. Genetic and imaging studies identified a few specific instances of translational regulation, including regional control of POS-1 translation[13–16] and regulation of other maternal transcripts [17–20], but these gene-by-gene studies do not reveal the global landscape of translational regulation in early embryos. Bulk ribosome profiling studies in *C. elegans* embryos have provided insights into translational regulation during embryogenesis[21,22], but these studies lacked temporal resolution due to the challenge of collecting staged embryo populations, and would average out any stage-specific translational regulation. In this work, we measured mRNA translation in precisely staged *C. elegans* embryos using a recent innovation, ribosome profiling via isotachophoresis (Ribo-ITP)[23] . Ribo-ITP employs a custom designed microfluidic chip that concentrates and size-

57 selects ribosome-protected RNA fragments using on-chip isotachophoresis[24] . This approach
58 enables highly efficient recovery of ribosome footprints from minimal input material. Ribo-ITP
59 has allowed extraction of ribosome footprints from single human cells and single mouse
60 embryos, representing a ~10,000-fold increase in sensitivity compared to earlier bulk ribosome
61 footprinting approaches[25,26]. Adapting Ribo-ITP to *C. elegans* embryos allowed us to overcome
62 the challenge of rapid and asynchronous embryonic development, which precludes large-scale
63 collections of staged embryos. Here, we applied Ribo-ITP and low-input RNA-seq to analyze
64 the first three cell divisions of *C. elegans* embryogenesis, revealing transcriptome-wide
65 changes in translation of mRNA at the one-, two-, four-, and eight-cell stages of *C. elegans*
66 embryos.

67 Translational landscapes in early embryos are significantly influenced by maternally deposited
68 RNA-binding proteins[27]. Many of these proteins, when mutated, cause maternal-effect lethality
69 and/or alter blastomere cell fates[28–31]. By analyzing translational changes in an RNA-binding
70 protein mutant we identified stage-specific regulation of hundreds of transcripts by OMA-1[31], a
71 translational repressor implicated in oocyte development[32–34] and early
72 embryogenesis[13,18,35,36]. These findings expand our understanding of OMA-1's regulatory
73 targets during early development in *C. elegans* and contribute to our knowledge of the influence
74 of maternal RNA-binding proteins on stage-specific translation during early embryogenesis.

2. Results

2.1. Low-input RNA-seq and Ribosome Profiling

We focused on the first three cell divisions of *C. elegans* embryogenesis, a period when the progenitors of all three germ layers are established. For each stage, we hand-dissected and flash-froze pools of nine precisely staged embryos for ribosome profiling (Ribo-ITP) or RNA-seq experiments (Figure 1A). Although we were able to obtain ribosome footprints from single embryos in pilot experiments, we found that using pools of nine embryos provided superior footprinting depth compared to using one embryo.

For each developmental stage, we obtained at least two high-quality Ribo-ITP replicates, which showed reads predominantly mapping to the coding sequence (CDS) region (Figure 1B) and characteristic enrichments at the start and stop sites (Figure 1C). Furthermore, these CDS-mapped reads exhibited the expected footprint size of approximately 30 nucleotides, typical of ribosome profiling experiments using MNase digestion (Figure S1A). After filtering and quality control, we obtained 4,905 genes that showed robust ribosome occupancy reads(methods). We observed strong replicate-to-replicate correlation between the number of ribosome footprints mapping to coding regions (Spearman rank correlation $\rho > 0.85$ $P < 2 \times 10^{-16}$), supporting the method's reproducibility (Figure 1D-G and Figure S1B). Clustering analysis, using multidimensional scaling, revealed global similarity of translational profiles obtained in replicate experiments, with the exception of one outlier (Figure S1C). Taken together, these metrics indicate technical robustness and reproducibility of our Ribo-ITP measurements.

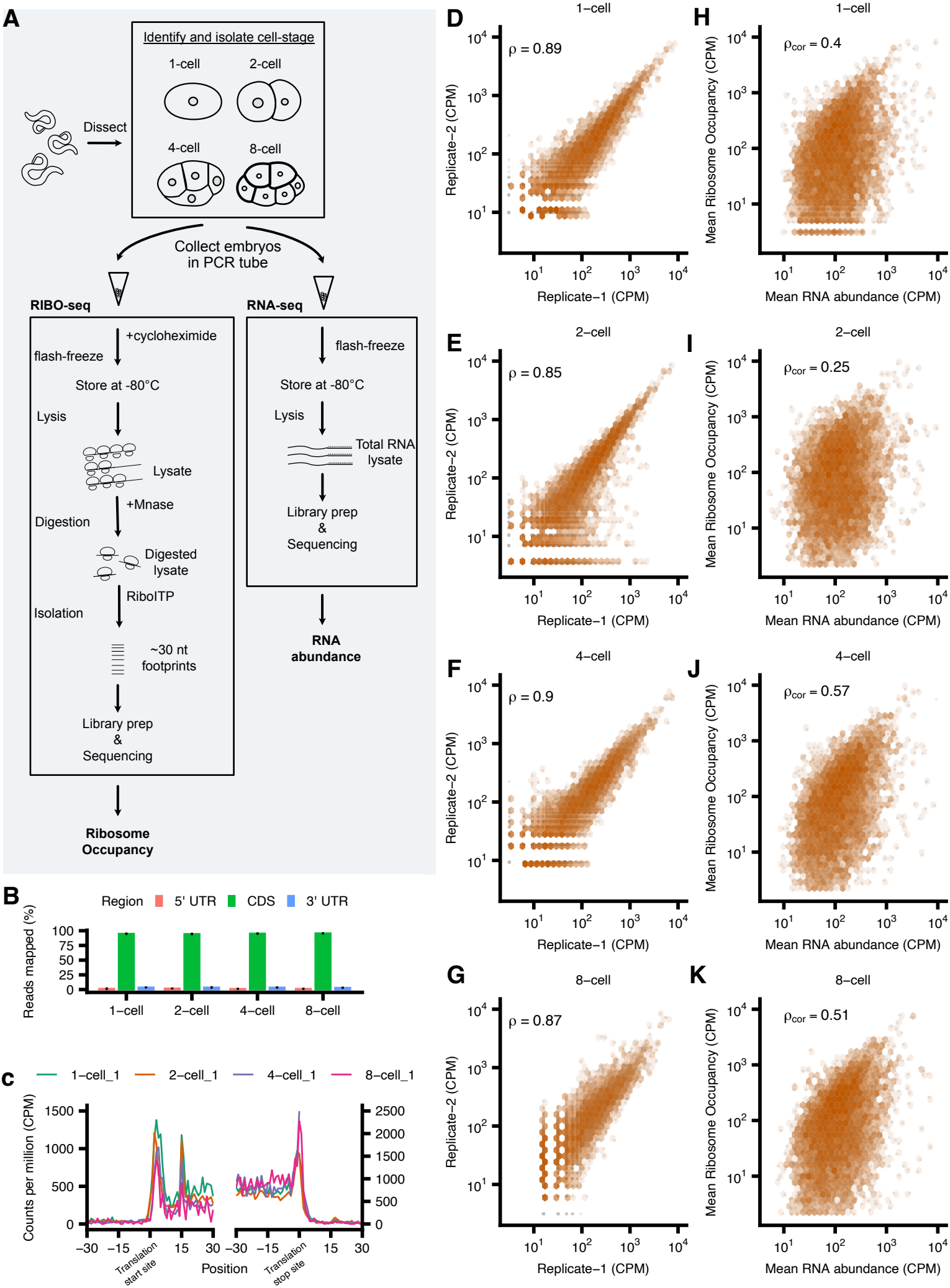
A
Identify and isolate cell-stage
1-cell
2-cell
4-cell
8-cell
Dissect
Collect embryos in PCR tube
RIBO-seq
RNA-seq
+cycloheximide
flash-freeze
Store at -80°C
Lysis
Lysate
+Mnase
Digestion
Digested lysate
RiboITP
Isolation
~30 nt footprints
Library prep & Sequencing
Ribosome Occupancy
flash-freeze
Store at -80°C
Lysis
Total RNA lysate
Library prep & Sequencing
RNA abundance
B
Region
5' UTR
CDS
3' UTR
Reads mapped (%)
1–cell
2–cell
4–cell
8–cell
C
1–cell_1
2–cell_1
4–cell_1
8–cell_1
Counts per million (CPM)
Translation start site
Position
Translation stop site
D
1–cell
ρ = 0.89
Replicate–2 (CPM)
Replicate–1 (CPM)
E
2–cell
ρ = 0.85
F
4–cell
ρ = 0.9
G
8–cell
ρ = 0.87
H
1–cell
ρcor = 0.4
Mean Ribosome Occupancy (CPM)
Mean RNA abundance (CPM)
I
2–cell
ρcor = 0.25
J
4–cell
ρcor = 0.57
K
8–cell
ρcor = 0.51

Figure 1: Low-input RNA-seq and Ribosome Profiling (A) Adult *C. elegans* were dissected to obtain embryos at 1-cell, 2-cell, 4-cell, and 8-cell stages, which were then subjected to ribosome profiling (Ribo-ITP) and RNA-seq analysis. **(B)** Mapping of ribosome profiling reads to different genomic features (CDS, 5' UTR, 3' UTR) is presented for each stage. Error bars indicate the standard deviation. **(C)** Ribosome occupancy around the translation start and stop sites in a representative 1-cell, 2-cell,4-cell and 8-cell staged embryo. Translation start (or stop) sites are denoted by the position 0. Aggregated read counts (*y* axis) relative to the start (or stop) sites are plotted after A-site correction **(D-G)** Hexbin plot illustrating pairwise correlations of Ribo-seq data between representative replicates across developmental stages. Each axis displays log-scaled counts per million (CPM) of detected genes. The Spearman correlation is indicated in the left corner of the plots. Darker orange color indicates high density of points. **(H-K)** Pairwise correlation between ribosome occupancy and RNA abundance at the four stages of early *C. elegans* embryo development is presented. The mean cpm of ribosome occupancy is plot against the mean cpm of RNA abundance at each stage. p_{cor} is the corrected spearman correlation based on the reliability r (RNA) and r (Ribo) which are the replicate-to-replicate correlation (methods).

To estimate how efficiently the mRNA of a given gene is being translated, its ribosome occupancy needs to be normalized to its mRNA abundance, which we quantified using RNA-seq experiments on the same developmental stages as those analyzed by Ribo-ITP. We observed that variability between replicates increased as development progressed, with the mean correlation between replicates decreasing from $\rho = 0.92$ at the 1-cell stage to $\rho = 0.73$ at the 8-cell stage (Figure S1D-E). We attribute this increase in variability to three factors: the stochasticity of gene expression[37], the increasing complexity of later embryos (with multiple cell types present), and possible PCR duplication during RNAseq library preparation. Despite these issues, in our 8-cell RNAseq dataset we robustly detected genes known to be expressed at the 8-cell stage in *C. elegans*[8,38,39], verifying the accuracy of our RNA-seq data for capturing developmental progression (Figure S2A). Having collected the two key metrics – RNA abundance and ribosome occupancy – we are now equipped to answer how translation of maternal mRNA changes globally.

2.2. Stage-specific patterns of translational regulation in early embryogenesis

The strength of the correlation between mRNA abundance and ribosome occupancy can indicate the extent to which translation is regulated. If there were no translational regulation – that is, if the amount of mRNA translation were governed solely by mRNA abundance – then mRNA abundance and ribosome occupancy should correlate strongly. Strikingly, however, we observed a weak correlation between mRNA abundance and ribosome occupancy, indicating widespread regulation of translation (Figure 1H-K). Furthermore, the correlation between ribosome occupancy and RNA-seq exhibited dynamic changes across early embryonic stages. Starting with a moderate correlation at the 1-cell stage ($\rho = 0.361$, $p < 2e\text{-}16$; $\rho_{cor} = 0.4$; Figure 1H), it decreased to a weak correlation at the 2-cell stage ($\rho = 0.220$, $p < 2e\text{-}16$; $\rho_{cor} = 0.25$; Figure 1I). The correlation then strengthened again during the 4-cell stage ($\rho = 0.502$, $p < 2e\text{-}16$; $\rho_{cor} = 0.57$; Figure 1J) and 8-cell stage ($\rho = 0.417$, $p < 2e\text{-}16$; $\rho_{cor} = 0.51$; Figure 1K). This pattern, particularly the sharp drop at the 2-cell stage followed by recovery at the 4-cell stage, suggests that the relationship between mRNA abundance and ribosome occupancy is developmentally regulated and may reflect stage-specific translational control mechanisms during early embryogenesis.

The observed low correlation between mRNA abundance and ribosome occupancy likely reflects the combined effect of technical variability, stage-specific translational regulation, and intrinsic diversity in mRNA translation efficiency (for example, due to differences in codon usage). We reasoned that previous ribosome profiling experiments from mixed-stage embryos would provide information regarding the relative contribution of the last two variables. Ribosome profiling experiments from mixed-stage datasets from pooled 1-cell to 200-cell stage[40] showed a strong correlation (Spearman rank correlation = 0.9, $p < 2e\text{-}16$; Figure S2B) between mRNA abundance and ribosome occupancy. This high correlation likely represents a

149 situation where intrinsic differences in mRNA properties (such as sequence features affecting
150 translation efficiency) predominate. In contrast, analyses from pooled 1-cell to 4-cell stage
151 embryos[21] revealed a more moderate correlation (Spearman rank correlation = 0.58, $p < 2e-$
152 16; Figure S2C). Our stage-specific correlations (Spearman rank correlations ranging from 0.22
153 to 0.50) were lower still, suggesting that beyond technical variability and intrinsic diversity in
154 mRNA translation efficiency, there may be substantial translational regulation that varies
155 between developmental stages. Importantly, this observation was not due to measurement
156 error, because when we accounted for variation across biological replicates (see methods), we
157 still observed a mean corrected correlation (ρ_{cor}) of 0.43 between ribosome occupancy and
158 RNA-seq across all four early embryonic stages. The progressive decrease in correlation
159 strength—from mixed-stage to pooled early stages to individual cell stages—provides evidence
160 that dynamic, stage-specific translational control mechanisms play an important role during
161 early *C. elegans* embryogenesis, beyond what can be explained by inherent differences in
162 mRNA properties alone.

163 We next wanted to identify which mRNAs are translationally regulated at each stage. We define
164 "translation efficiency" (TE) in alignment with its common usage in the literature[25,26,41–43] by
165 normalizing ribosome occupancy to mRNA abundance. TE provides a measure of the relative
166 rate of protein synthesis [25,44,45] and is an indicator of active translation for most endogenous
167 transcripts[25], despite some exceptions in specific instances where ribosome density is
168 decoupled from protein production (e.g., ribosome stalling[46,47]).

169 To assess developmentally regulated translation of maternal mRNAs, we conducted pairwise
170 differential expression analysis between subsequent stages of development, observing
171 changes in RNA abundance, ribosome occupancy and TE. We detected 179 and 40 mRNAs
172 whose TE increased (FDR < 0.2, log2FC > 1) or decreased (FDR < 0.2, log2FC > -1),
173 respectively, as embryos progressed from the 1-cell to the 2-cell stage (Figure 2A). From the

174 2-cell to the 4-cell stage we observed 30 and 11 mRNAs whose TE was relatively increased or
175 decreased, respectively (Figure 2B). We did not observe significant changes between the 4-
176 cell and 8-cell stages (Figure 2C), which could reflect both technical and biological factors. The
177 1-cell to 2-cell comparison represents a transition between two relatively uniform states, while
178 later stages involve multiple distinct cell types, potentially making stage-specific changes more
179 difficult to detect. Additionally, rapid and asynchronous cell divisions occurring from 6 to 8 to 12
180 cells in this system, and/or mixing of multiple distinct cell types within an 8-cell embryo, would
181 tend to dilute out cell-specific translational changes. Comparing 1-cell to 8-cell stages (Figure
182 S3A) revealed broader translational remodeling, with 421 genes showing increased TE and
183 296 showing decreased TE ($|\log_2 FC| > 1$, FDR < 0.1). The larger number of significant changes
184 detected when comparing 1-cell to 8-cell stages suggests that many transcripts undergo
185 gradual but consistent changes in TE across several cell cycles, some of which do not reach
186 statistical significance when comparing between neighboring stages (e.g., 4-cell vs. 8-cell). The
187 substantial number of differentially translated transcripts - affecting over 700 genes in total -
188 suggests a major reorganization of the translational landscape during early development. This
189 large-scale translational regulation likely reflects the transition from maternally provided
190 programs to stage-specific translation required for proper cell fate specification.

191

192

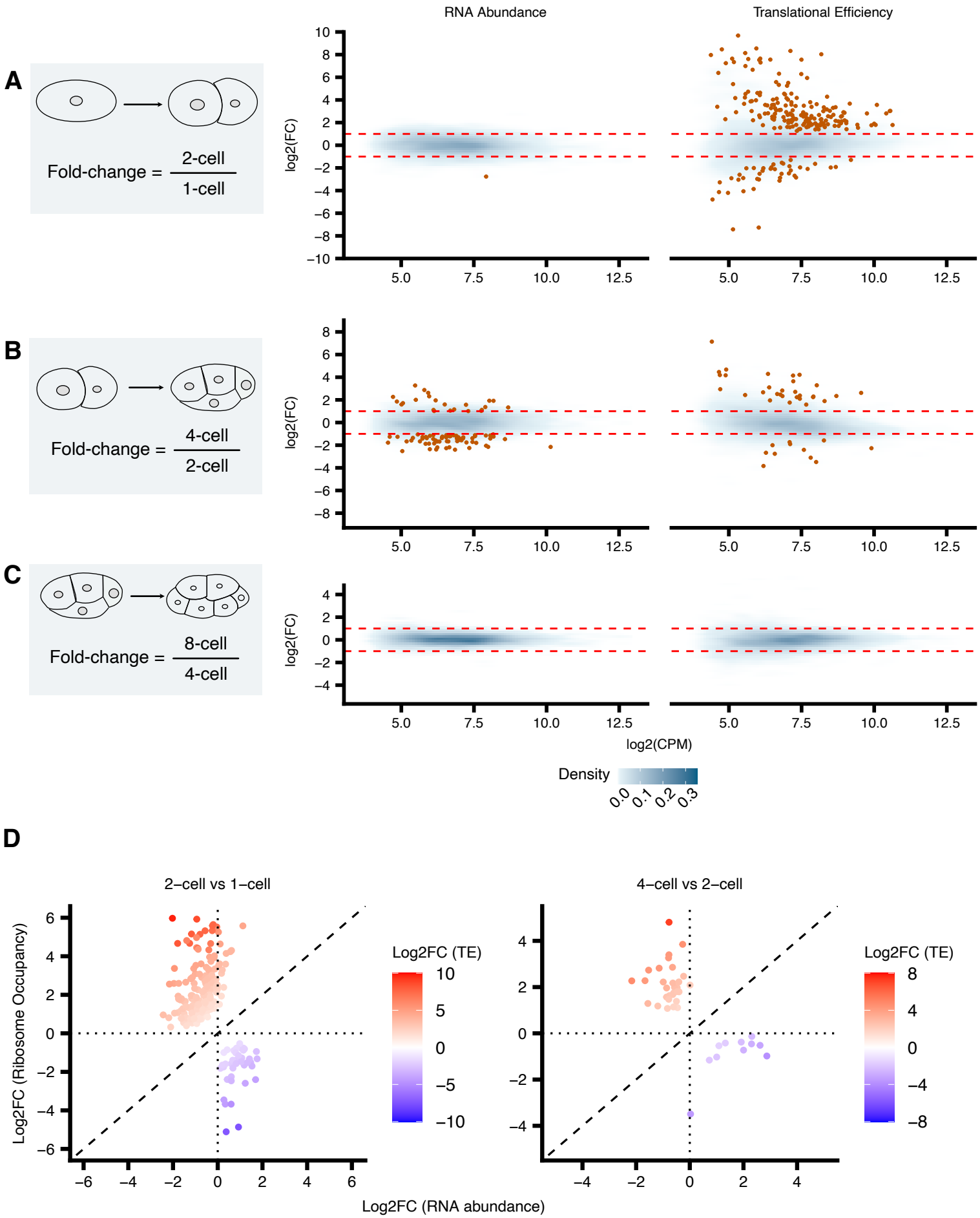
A
Fold-change = 2-cell / 1-cell
B
Fold-change = 4-cell / 2-cell
C
Fold-change = 8-cell / 4-cell
RNA Abundance
Translational Efficiency
log2(FC)
log2(CPM)
Density
0.0
0.1
0.2
0.3
D
2–cell vs 1–cell
4–cell vs 2–cell
Log2FC (Ribosome Occupancy)
Log2FC (RNA abundance)
Log2FC (TE)

Figure 2: Stage-specific patterns of translational regulation in early embryogenesis Mean difference plots comparing gene expression between sequential *C. elegans* embryonic stages **(A)**1-cell to 2-cell, **(B)** 2-cell to 4-cell, and **(C)** 4-cell to 8-cell. The log_2 fold change in RNA abundance and Translational efficiency (y-axis) is plotted against the mean of normalized counts (x-axis). Blue density plot represents the overall distribution of genes with the intensity corresponds to the density of points. The orange points indicate transcripts with significant expression changes (FDR < 0.2 and log_2FC >1 or < -1). **(D)** Scatter plot comparing the log2 fold change in ribosome occupancy against RNA abundance for genes with significantly altered translational efficiency. The color gradient represents the corresponding translational efficiency for each gene.

We next visualized the extent to which observed changes in TE were due to changes in ribosome occupancy (Figure S3B) vs. changes in mRNA abundance (Figure 2D). For most genes, the change in ribosome occupancy was larger than the change in mRNA abundance. An exception is a cluster of genes whose mRNAs increase 2 to 4-fold in abundance at the 4-cell stage without a corresponding increase in ribosome footprints (Figure 2D, blue points to the right of the origin in the right-hand plot). These apparent increases in mRNA abundance may reflect the compositional nature of RNA-seq and ribosome profiling[48], whereby degradation of a large number of transcripts[21,49,50] could artificially inflate the relative abundance of the remaining stable mRNAs. Taken together, we observe a large-scale stage-specific translationally efficiency changes that occur with limited changes in RNA-abundance.

We compared our normalized translational efficiency (see methods) against prior measurements by plotting our measured stage-specific TE values against the TE values reported by Quarto et al. (2021) and Lee et al. (2022). Our data demonstrate concordance with the translational regulation patterns reported by Quarto et al. (2021)[21] (Spearman rank correlation range from 0.54 to 0.64, $p < 2e-16$; Figure S3C), while showing weaker similarity to findings in Lee et al. (2022)[22] (Spearman rank correlation range from 0.36 to 0.42, $p < 2e-16$; Figure S3D). This alignment with Quarto et al. is expected, as their methodology specifically isolated ribosome profiling data from pooled early embryos, which more closely match our experimental strategy. In contrast, Lee et al. (2022)[22] analyzed a broader developmental

221 window (1-200 cells) as a single population, likely diluting stage-specific translational
222 signatures that are prominent in our narrowly defined developmental timepoint.

223 *2.3. Functional clustering reveals developmentally coordinated translational*
224 *programs*

225 We next asked whether functional groups of genes undergo coordinated translational
226 regulation across the 1-cell, 2-cell, 4-cell, and 8-cell stages. To compare stage-specific changes
227 in TE, we normalized the TE values to the 1-cell stage for all genes and centered the data by
228 subtracting the mean TE across all stages for each gene (see Methods). This preprocessing
229 step allowed us to highlight developmental stage-specific fluctuations in TE. To analyze
230 coordinated regulation across stages, we employed a group-based approach using k-means
231 clustering to categorize genes based on their TE patterns, resulting in nine distinct clusters
232 (Figure 3A). While a gene-by-gene statistical analysis can identify significantly changed
233 individual genes (Figure 2A-C), this clustering approach enhanced our ability to detect more
234 subtle patterns of coordinated regulation across developmental stages by analyzing groups of
235 genes that underwent similar changes. We observed that most of the changes in TE occurred
236 due to changes in ribosome occupancy, while mRNA abundance was generally stable through
237 these cell stages (Figure 3B). This approach enabled us to identify and characterize groups of
238 genes with similar translational regulation patterns. We observed enrichment of unique
239 biological functions in each cluster (Figure 3C). The clusters with opposing translational
240 trajectories showed particularly distinct functional specializations. For example, in Cluster I,
241 which exhibits progressive translational repression from the 1-cell to 8-cell stage, we observed
242 enrichment of P-granule components and regulators of TOR signaling, perhaps suggesting a
243 transition from oocyte to embryonic development where TOR-mediated nutrient sensing
244 becomes less critical as the embryo shifts to a developmental program less dependent on
245 external nutrient availability. In contrast, Cluster IX, which shows strong translational activation

246 across development, is enriched for transcription factors and chromatin regulators, suggesting
247 that the embryo is preparing for zygotic genome activation by increasing the translation of
248 proteins needed for transcriptional machinery before widespread zygotic transcription begins.

249 We next checked whether the patterns we observed were consistent with prior knowledge.
250 Translational regulation has been shown to influence Wnt signaling[18], E3 ubiquitin ligase-
251 mediated protein degradation[36], and transcription factor activity[51–53]. We observed that the Wnt
252 protein MOM-2 (cluster VIII) was translationally repressed at the 1-cell and 2-cell stage and
253 increased in TE by ~10-fold at the 4-cell stage (Figure S4A), consistent with the onset of its
254 protein expression at the 4-cell stage[18]. The transcription factor PAL-1 (cluster VIII; Figure 3A)
255 had a TE 4.5 times lower than that of the average gene at the one-cell stage, with rapid
256 increases at the two- and four-cell stages before leveling off at the 8-cell stage (Figure S4A).
257 Consistent with this, PAL-1 was previously shown to be expressed beginning at the 4-cell stage,
258 although *pal-1* mRNAs are maternally deposited[52,54]. Thus, for these examples, our
259 transcriptome-wide data are consistent with prior knowledge from gene-by-gene studies.

260 NEG-1 (cluster I) translation was proposed to be regulated by mRNA binding proteins including
261 MEX-5, MEX-3, POS-1, GLD-2, and GLD-3[16]. We observed a progressive decrease ribosome
262 occupancy for cluster I transcripts including *neg-1* from 1-cell to 8-cell stages, with a limited
263 change in overall RNA levels (Figure 3B). Correspondingly, we found reduced TE for *neg-1* at
264 4-cell and 8-cell stages (Figure S4A), earlier than the previously observed protein degradation
265 at the 10-cell stage[16].

266 Finally, the Nanos homolog NOS-2 (cluster VI), whose mRNA is maternally deposited but not
267 translated until the 28-cell stage (and then only in the germline founder cell P4)[13,22,55], exhibited
268 very low TE at all the stages we analyzed (Figure S4A), consistent with its strong translational
269 repression. Taken together, our genome-wide translational profiling data mirror known

270 regulatory dynamics of key developmental factors, demonstrating the sensitivity and reliability
271 of our approach in capturing translational regulation of maternal mRNAs.

272 To further validate our findings and explore potentially uncharacterized changes in protein
273 expression, we examined several key developmental proteins that were identified as being
274 translationally regulated in our dataset. We identified the Wnt pathway receptor tyrosine kinase
275 CAM-1 (Cluster IX) as translationally upregulated beginning at the 2-cell stage (Figure S4A),
276 though its protein expression had only been previously observed in later stages[56] . Initially, we
277 detected only punctate localization of an endogenous CAM-1::mNG fusion in live early embryos
278 (Figure S4B-C) that differed from CAM-1's expected localization at cell-cell contacts[56] .We
279 speculated that newly translated CAM-1::mNG might be difficult to detect via live imaging due
280 to slow fluorescent protein maturation at the standard *C. elegans* culture temperature of 20°C.
281 To overcome this limitation, we fixed embryos and incubated them at 37°C to allow fluorescent
282 protein maturation before imaging (see Methods). This approach revealed previously
283 unobservable CAM-1 protein signals at early stages, specifically at cell-cell contacts beginning
284 at the 4-cell stage (Figure S4C), consistent with its increase in TE in our Ribo-ITP data. We
285 extended this analysis to LAG-1 (Cluster IX), a Notch pathway transcription factor, which was
286 visible in the nucleus from the 1-cell stage in live imaging but only showed an apparent increase
287 in signal intensity from 1-cell to 4-cell stages after fixation and fluorophore maturation (Figure
288 S4D). Interestingly DSH-2 (Cluster VIII), another Wnt pathway component predicted to
289 increase from 2-cell to 4-cell stages, showed detectable signal increases in both live and fixed
290 conditions (Figure S4E), suggesting that perhaps fluorophore maturation can vary depending
291 on the fusion protein. Collectively, these results demonstrate that key components of
292 developmental signaling pathways are translated earlier than previously appreciated, and that
293 Ribo-ITP can identify previously undetected protein expression in early *C. elegans* embryos.

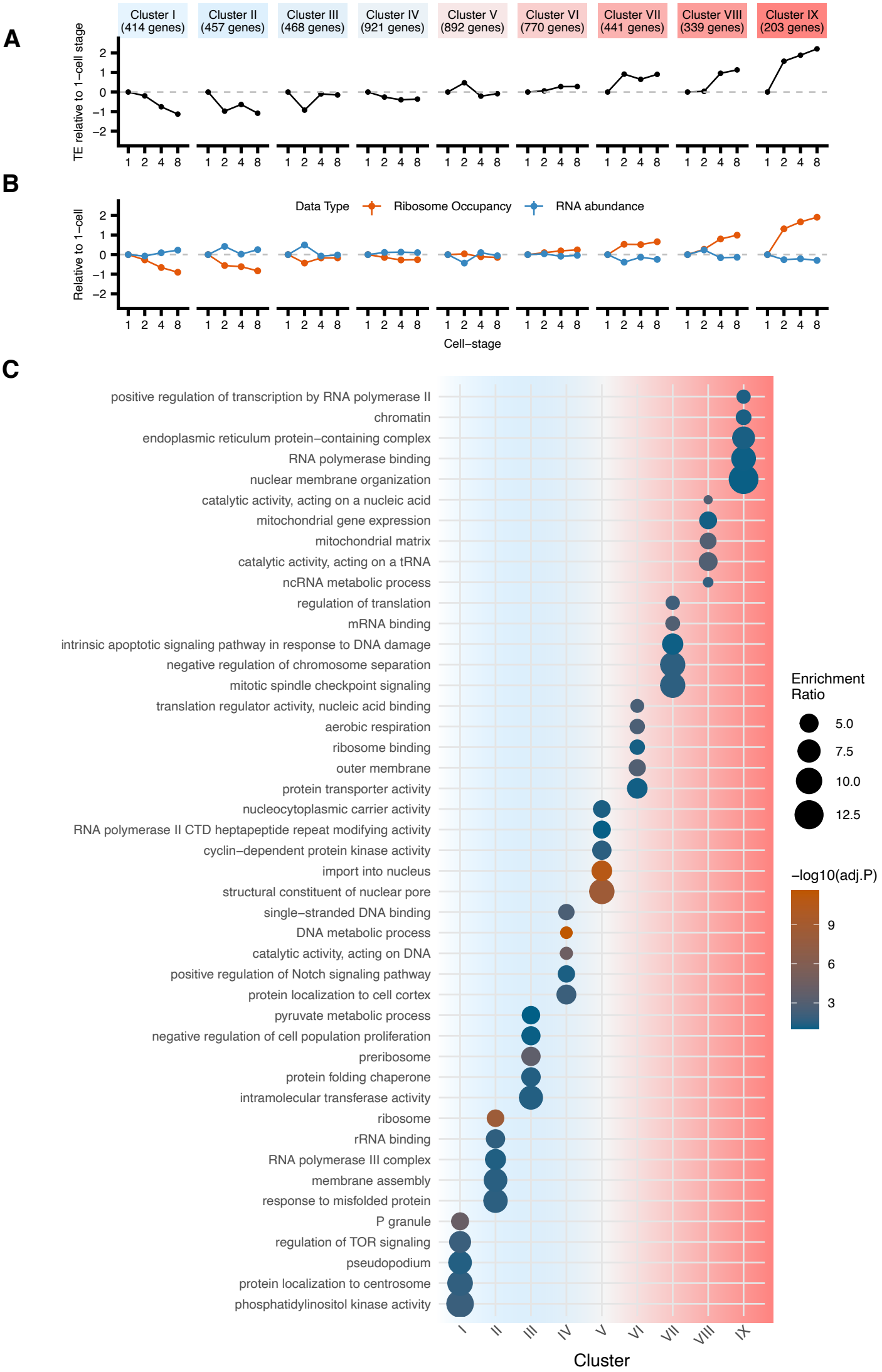
A
Cluster I (414 genes)
Cluster II (457 genes)
Cluster III (468 genes)
Cluster IV (921 genes)
Cluster V (892 genes)
Cluster VI (770 genes)
Cluster VII (441 genes)
Cluster VIII (339 genes)
Cluster IX (203 genes)
TE relative to 1−cell stage
B
Data Type
Ribosome Occupancy
RNA abundance
Relative to 1−cell
Cell−stage
C
positive regulation of transcription by RNA polymerase II
chromatin
endoplasmic reticulum protein−containing complex
RNA polymerase binding
nuclear membrane organization
catalytic activity, acting on a nucleic acid
mitochondrial gene expression
mitochondrial matrix
catalytic activity, acting on a tRNA
ncRNA metabolic process
regulation of translation
mRNA binding
intrinsic apoptotic signaling pathway in response to DNA damage
negative regulation of chromosome separation
mitotic spindle checkpoint signaling
translation regulator activity, nucleic acid binding
aerobic respiration
ribosome binding
outer membrane
protein transporter activity
nucleocytoplasmic carrier activity
RNA polymerase II CTD heptapeptide repeat modifying activity
cyclin−dependent protein kinase activity
import into nucleus
structural constituent of nuclear pore
single−stranded DNA binding
DNA metabolic process
catalytic activity, acting on DNA
positive regulation of Notch signaling pathway
protein localization to cell cortex
pyruvate metabolic process
negative regulation of cell population proliferation
preribosome
protein folding chaperone
intramolecular transferase activity
ribosome
rRNA binding
RNA polymerase III complex
membrane assembly
response to misfolded protein
P granule
regulation of TOR signaling
pseudopodium
protein localization to centrosome
phosphatidylinositol kinase activity
Cluster
Enrichment Ratio
5.0
7.5
10.0
12.5
−log10(adj.P)
9
6
3

Figure 3: Functional clustering reveals developmentally coordinated translational programs. K-means clustering was performed on normalized TE values for all genes, with data centered by subtracting the mean TE across all stages for each gene. This analysis yielded 9 distinct clusters. **(A)** The line plot displays 1-cell stage subtracted TE values (y-axis) across developmental stages (x-axis). Clusters are color-coded based on broad TE patterns: blue for repression and red of activation. Error bars represent the standard error of TE values for all genes within each cluster. **(B)** Line plot showing the centered-log ratio of ribosome occupancy (orange) and RNA abundance (blue) at developmental stages relative to the 1-cell stage. **(C)** The dot plot visualizes Gene Ontology (GO) enrichment analysis for the identified clusters. The y-axis shows enriched GO terms, while the x-axis represents clusters. Dot size indicates enrichment ratio, and color intensity reflects the adjusted p-value of enrichment.

2.4. *P-granule localization occurs only after translational repression*

The distinction between germline and somatic cell lineages is a fundamental aspect of animal development. To explore how translation is regulated during development of the germline lineage, we integrated our TE measurements with existing single-cell RNAseq[8] and *in situ* hybridization data[40,57] that revealed the localization of transcripts in specific cells or subcellular regions. Our analysis revealed significantly lower translation in germline-localized transcripts compared to somatic transcripts across early development (Figure 4A; two-cell: -0.896 vs 0.792; four-cell: -1.44 vs 0.912; eight-cell: -1.34 vs 1.16; all stages $p < 0.001$).

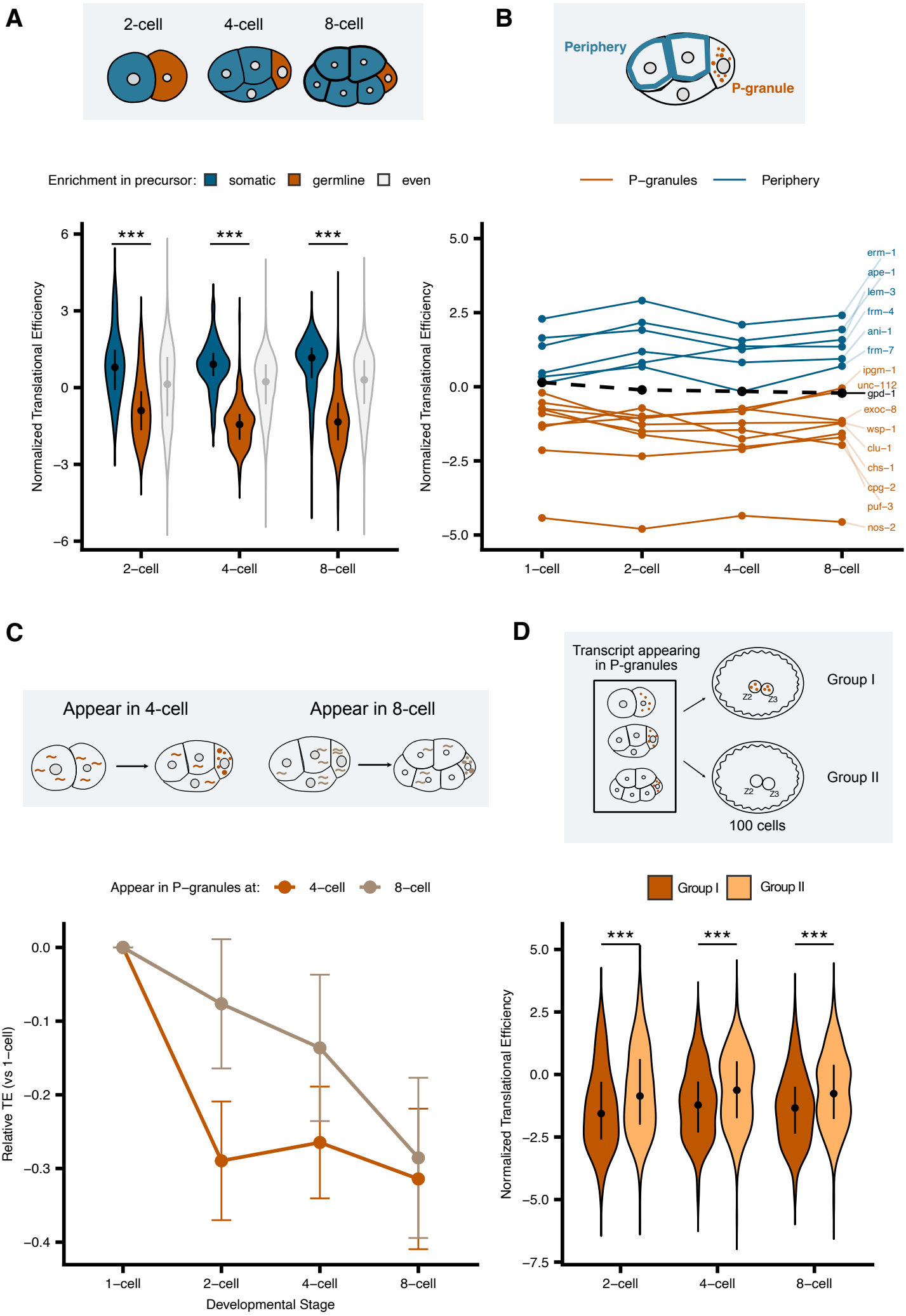
A
2-cell
4-cell
8-cell
B
Periphery
P-granule
Enrichment in precursor: somatic germline even
P−granules Periphery
Normalized Translational Efficiency
***
2−cell
4−cell
8−cell
1−cell
erm−1
ape−1
lem−3
frm−4
ani−1
frm−7
ipgm−1
unc−112
gpd−1
exoc−8
wsp−1
clu−1
chs−1
cpg−2
puf−3
nos−2
C
Appear in 4-cell
Appear in 8-cell
Appear in P−granules at: 4−cell 8−cell
Relative TE (vs 1−cell)
Developmental Stage
D
Transcript appearing in P-granules
Group I
Group II
Z2
Z3
100 cells
Group I Group II

Figure 4: P-granule localization occurs after translational repression (A) Violin plots illustrating the distribution of normalized translational efficiency for transcripts enriched in somatic and germline precursor cells (enrichment data from Tintori et al [8]) of early *C. elegans* embryos. The width of each violin represents the probability density of efficiency values. Median normalized translational efficiency is indicated by a dot, with error bars showing the first (Q1) and third (Q3) quartiles. **(B)** Line plot showing the mean normalized translational efficiency of transcripts localized in the cell periphery and P-granules (based on smFISH data from Parker et al[57] and Winkenbach et al [19]) across embryonic stages from 1-cell to 8-cell. This plot compares the translational efficiency trends of these two transcript populations throughout early embryonic development. **(C)** Translational efficiency relative to 1-cell stage for transcripts that transition into P-granules (P-granule localization identified in Scholl et al [40]). Orange line shows transcripts that first appear in P-granules at the 4-cell stage (n=81), brown line shows transcripts first appearing at 8-cell stage (n=43). Error bars represent standard error of the mean. **(D)** Translational efficiency of P-granule transcripts based on their maintenance in primordial germ cells (Z2/Z3). Group I transcripts remain associated with P-granules through primordial germ cell development (n=163), while Group II transcripts show transient P-granule association (n=277) (localization identified in Scholl et al). Violin plots show distribution of translational efficiency values, with median and quartiles indicated. Asterisks denote statistical significance between groups (*$p < 0.05$, **$p < 0.01$, ***$p < 0.001$, Wilcoxon rank-sum test).

P granules, which are predominantly found in the germline, have been proposed as sites where translationally repressed transcripts accumulate. When we compared transcripts that were shown to localize to the cell periphery versus in P granules [19,57], we observed that P granule localized transcripts showed low TE while cell periphery transcripts showed high TE. To further validate this observation, we analyzed 458 P-granule-localized transcripts from a prior study[40], which confirmed their globally reduced translational efficiency across development (Figure S5A; median TE at 2-cell: -1.51, 4-cell: -1.20, 8-cell: -1.14). This suggested that translational repression is a specific property of P-granule-associated transcripts.

Since P granules are associated with translational repression, their presence in the germline founder cells could, in principle, explain the reduced translation of germline-enriched transcripts. However, when we examined the overlap between P-granule transcripts (obtained from Scholl et al [40]) and germline-enriched genes (obtained from Tintori et al [8]) we found minimal overlap with only 2 out of 245 P-granule transcripts overlapping with the 53 germline-enriched genes (Fisher's exact test, $p = 1.0$, Figure S5B and Table S3). The overlap did increase during development, with 31/326 P-granule transcripts overlapping with 160 germline-enriched genes at the four-cell stage ($p < 0.001$) and 125/389 P-granule transcripts overlapping with 496 germline-enriched genes at the eight-cell stage ($p < 0.001$; Figure S5B). This progressive enrichment occurs in concert with more transcripts becoming germline-enriched

349 as development proceeds and likely reflects selective degradation these transcripts in somatic
350 lineages [21,50,58] rather than active localization to P-granules in the germline.

351 To further investigate the temporal relationship between P-granule localization and translational
352 repression, we analyzed transcripts that were shown to transition from non-P-granule to P-
353 granule localization during early embryogensis[53]. While previous studies established that P-
354 granules are not required for translational repression and that poorly translated mRNAs can
355 accumulate in P-granules, these analyses were limited by either focusing on select
356 transcripts[57], or using pooled embryos across multiple developmental stages[22], potentially
357 masking stage-specific dynamics. By analyzing 81 transcripts that transition from non-P-
358 granule to P-granule localization[53] between the 2-cell and 4-cell stages, we observed a
359 significant drop in TE between the 1-cell and 2-cell stages (median difference = -0.4, Wilcoxon
360 rank test, $P = 6.28 \times 10^{-5}$), before their P-granule localization, with no significant change in TE
361 coinciding with their movement into P-granules ($p = 0.6344$; Figure S5C and 4C). Thus, for
362 these transcripts, translational repression precedes P-granule localization. A second class of
363 transcripts showed P-granule localization beginning at the 8-cell stage[53]. These 70 transcripts
364 underwent a more gradual decline in TE, but this decline still started before P-granule
365 localization was observed (Figure 4C). We conclude that across the transcriptome,
366 translational repression consistently precedes P-granule localization during early
367 embryogenesis.

368 Examining P-granule localization across a broader range of developmental time, a previous
369 analysis identified two groups of P-granule transcripts. Group I maintains stable P-granule
370 association throughout primordial germ cell development, while Group II shows transient P-
371 granule localization during early embryogenesis[40]. Group I mRNAs showed consistently lower
372 translational efficiency compared to Group II transcripts across the stages we examined (8-cell
373 medians: -1.34 vs -0.765, $p = 2.21e-5$, Figure 4D). GO enrichment analysis from a previous

374 study showed that Group I transcripts were enriched for terms related to germline development
375 and reproduction, whereas Group II transcripts were enriched for terms related to metabolic
376 processes[40], suggesting distinct functional roles for these transcript classes. Together, these
377 findings indicate that translational repression in the germline occurs independently of P-granule
378 association and reveals that P-granules contain functionally distinct transcript populations with
379 different degrees of translational control.

380 ***2.5. OMA-1 Regulates Translational Efficiency in a Stage-Specific Manner***

381 Our analysis to this point has revealed dynamic changes in TE across developmental stages,
382 which correlate with cell lineage and subcellular mRNA localization. In *C. elegans,* several
383 maternally deposited RNA-binding proteins contribute to spatiotemporally regulated protein
384 expression during early embryonic development[18,27,36,59]. To identify which RNA-binding
385 proteins are most likely to directly regulate translation at the stages we analyzed, we used
386 linear regression analysis (Table S4) to ask how strongly TE correlated with experimental RNA-
387 protein binding data (OMA-1 [34] and GLD-1 [60]) or the presence of binding motifs in transcripts
388 (POS-1 [61], MEX-3 [62], GLD-1 [60] and LIN-41 [32]) (Figure S6; Methods). OMA-1 binding showed
389 the strongest correlation with translational repression (Figure S6). OMA-1-bound transcripts
390 showed significantly lower TE in the 1-cell stage (median TE: -0.823 vs 0.254; Wilcoxon rank
391 test, p = 8.09e-62) and 2-cell stage (median TE: -0.235 vs 0.177; p = 1.05e-8) (Figure 5A). This
392 repressive effect weakened in later stages, becoming non-significant at the 4-cell stage
393 (median TE: 0.162 vs 0.180; Wilcoxon rank test, p = 0.283) and showing a slight reversal at
394 the 8-cell stage (median TE: 0.293 vs 0.128; p = 0.0171) (Figure 5A). This developmental
395 progression of TE effects correlates with the known degradation of OMA-1 during the 2-cell
396 stage (Figure 5B). Other RNA-binding proteins showed distinct patterns: POS-1, GLD-1, and
397 LIN-41 binding motifs were associated with increased TE across all stages (1-cell stage:
398 coefficients = 0.19, 0.22, and 0.32 respectively, all p < 1e-4), while MEX-3 showed a mild
399 correlation with repression that was only significant at the 2-cell stage (coefficient = -0.10, p =
400 0.027; Figure S6).

401

402

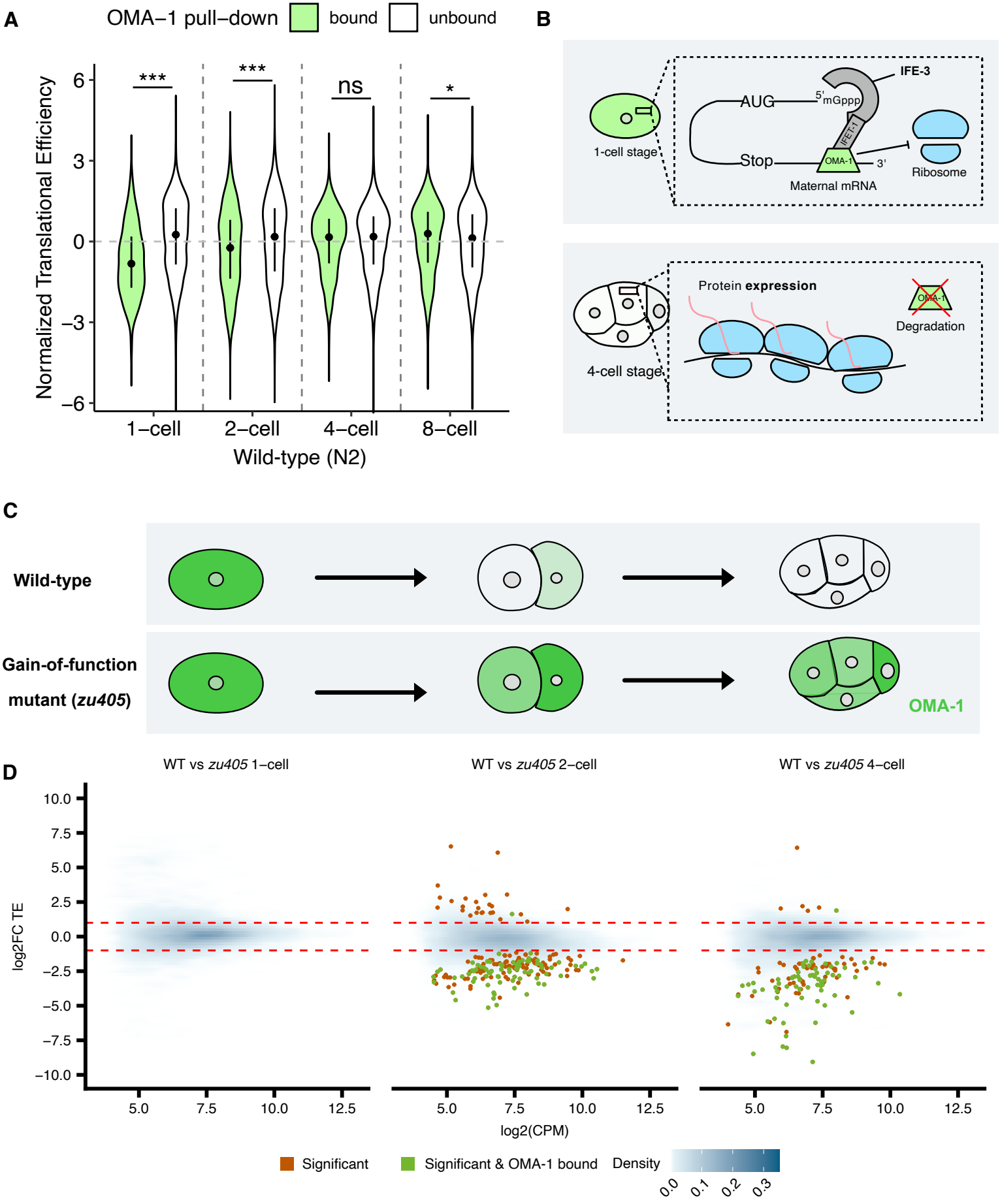
A
OMA−1 pull−down
bound
unbound
Normalized Translational Efficiency
***
***
ns
*
1−cell
2−cell
4−cell
8−cell
Wild-type (N2)
B
1-cell stage
AUG
Stop
5' mGppp
IFE-3
IFE-1
OMA-1
3'
Maternal mRNA
Ribosome
4-cell stage
Protein expression
Degradation
C
Wild-type
Gain-of-function mutant (zu405)
OMA-1
D
WT vs zu405 1−cell
WT vs zu405 2−cell
WT vs zu405 4−cell
log2FC TE
log2(CPM)
Significant
Significant & OMA-1 bound
Density

Figure 5: OMA-1 Regulates Translational Efficiency in a Stage-Specific Manner (A) Violin plots in illustrate the distribution of normalized translational efficiency for OMA-1-bound (green) and unbound (white) transcripts (as identified by Spike et al [34]) across four early *C. elegans* embryonic stages (1-cell, 2-cell, 4-cell, and 8-cell), identified from previous identified from previous OMA-1 associated RNA microarray data. The width of each violin represents the probability density of efficiency values. **(B)** Schematic diagram depicting OMA-1's regulatory mechanism in early embryogenesis, showing OMA-1 inhibiting translation of maternal transcripts at the 1-cell stage, followed by its degradation by the 4-cell stage, which allows translation of previously repressed transcripts. **(C)** Illustrates the difference in OMA-1 degradation between wild-type and *zu405* mutant embryos. **(D)** A pairwise comparison of translational efficiency between wild-type and mutant at each stage. This is represented as $\log_2$ fold change in translational efficiency (y-axis) against the mean of normalized counts (x-axis). A blue density plot represents the overall distribution of genes, with intensity corresponding to point density. Orange points indicate transcripts with significant expression changes (FDR < 0.2), while green points highlight known OMA-1-bound transcripts (as identified by Spike et al [34]) with significant changes in translational efficiency.

Given OMA-1's striking repressive signature and previous studies showing its role in translationally regulating several specific transcripts during oocyte maturation and early embryogenesis[13,18,34–36,59,63], we sought to globally characterize OMA-1's effects on translation during early embryonic development. We carried out Ribo-ITP and RNA-seq experiments using a gain-of-function mutant of *oma-1(zu405)* (Figure S7). This mutant harbors a P240L mutation preventing timely OMA-1 degradation at the two- and four-cell stages and resulting in dominant, temperature-sensitive embryonic lethality[31] (Figure 5C). We compared TE in *oma-1(zu405)* embryos, raised at the non-permissive temperature, to wild-type embryos (Figure 5D). At the one-cell stage, there were no significant differences ($|\log_2 FC| > 1$ and FDR < 0.2), as expected given OMA-1's presence in both. However, at later stages, we observed widespread aberrant translational repression in the *zu405* mutant, affecting 205 transcripts at the 2-cell stage and 125 at the 4-cell stage ($|\log_2 FC| > 1$ and FDR < 0.2; Figure 5D). Interestingly, only a subset of these repressed transcripts (79 at 2-cell and 66 at 4-cell stages) were among the 815 previously identified OMA-1-associated transcripts from adult worms[34] (green points in Figure 5D). This discrepancy likely reflects both embryo-specific OMA-1 binding not captured in the adult-based pulldown data and indirect regulation through OMA-1's effects on other RNA regulatory factors. Surprisingly, we also observed relative upregulation ($\log_2 FC > 1$ and FDR <0.2) of a small number of transcripts in *oma-1(zu405)* mutants at the 2-cell (26) and 4-cell (6) stages, respectively. These findings highlight the complex and far-reaching effects of OMA-1 on the translational landscape of early *C. elegans* embryos, revealing both direct and potentially cascade effects on gene regulation.

436 ***2.6. Failure of translational remodeling in oma-1(zu405) reveals diverse regulatory***
437 ***mechanisms***

438 While our initial analysis revealed global TE changes between wild-type and *oma-1(zu405)*
439 embryos at specific stages, we next examined how the temporal progression of translation was
440 altered within the mutant embryos themselves. The *oma-1(zu405)* mutant is 100% embryonic
441 lethal at the non-permissive temperature; embryos fail to specify tissues properly and do not
442 undergo embryonic morphogenesis[31]. By analyzing stage-to-stage transitions in *oma-*
443 *1(zu405)*, we sought to understand OMA-1's role in orchestrating the normal developmental
444 program of translational control. Strikingly, there were only 35 genes that changed significantly
445 ($|\log_2 FC|>1$ and FDR <0.2) in TE from the 1-cell to 2-cell stage and only 3 genes from the 2-
446 cell to 4-cell stage in *oma-1(zu405)* (Figure 6A), in contrast to wild-type embryos where
447 hundreds of genes undergo changes in TE between these stages (Figure 2A). In contrast to
448 wild-type embryos, where OMA-1-bound transcripts showed a progressive increase in
449 translational efficiency (TE) over time, in *zu405* mutants the below-average TE for OMA-1-
450 bound transcripts was maintained (Figure S7F, compare to Figure 5A). The median normalized
451 TE of OMA-1 bound transcripts was significantly lower than that of unbound transcripts in 4-
452 cell *oma-1(zu405)* embryos (-0.122 bound vs 0.212 unbound, p = 1.19e-11), in contrast to wild-
453 type where this difference was not significant (0.162 bound vs 0.180 unbound, p = 0.283). Thus,
454 the failure to degrade OMA-1 in the mutant appears to stall the developmental program,
455 preventing the normal translational remodeling that should occur by the 2-cell and 4-cell stages.

456 To further elucidate which genes might contribute to this developmental stalling, we compared
457 the log fold change in TE between wild-type and mutant embryos for transcripts that showed
458 significant TE changes. Intriguingly, we found that transcripts exhibiting increased TE from the
459 1-cell to 2-cell stage in wild-type embryos, but no significant change in mutants, were enriched
460 for previously identified OMA-1-bound transcripts (136 out of 179 transcripts; Figure 6B, green

points). This pattern suggests that many translationally upregulated transcripts at the 2-cell stage are direct OMA-1 targets that are aberrantly repressed in *zu405*. Conversely, among the transcripts that decreased in TE from 1-cell to 2-cell stage in wild-type embryos but remained unchanged in mutants, none of the downregulated genes was a known OMA-1 binder (Figure 6B). A similar pattern was observed for the 2-cell to 4-cell transition (Figure 6D). We note that changes in mRNA abundance were limited across all conditions, indicating that the majority of these changes in TE arise due to altered ribosome occupancy (Figure S8D and S8E). Additionally, we identified several potential non-OMA-1-bound transcripts with altered TE in mutants (Figure 6A and 6B). These changes likely reflect indirect effects mediated by OMA-1's regulation of transcripts encoding RNA regulatory factors.

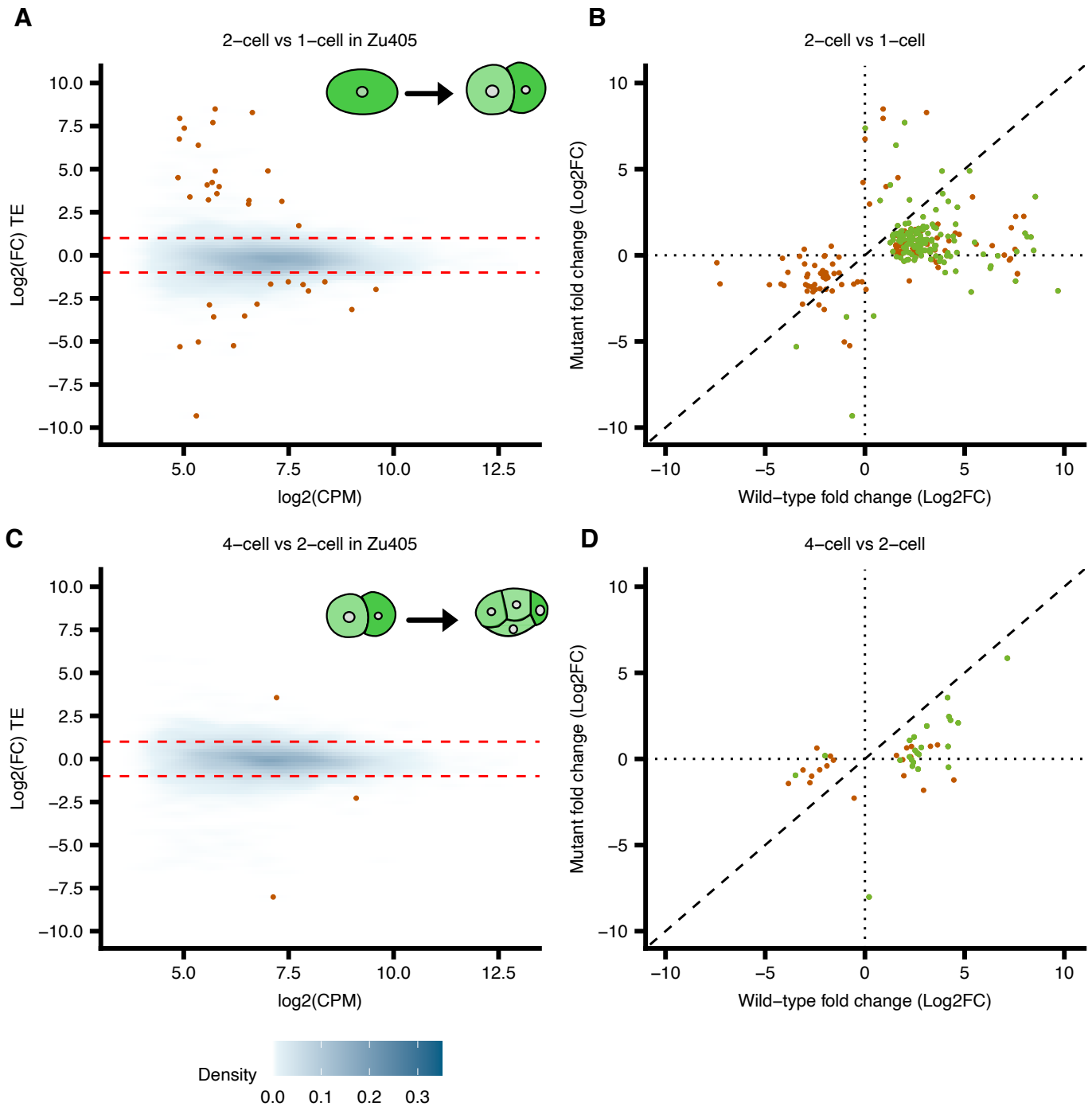
A
2–cell vs 1–cell in Zu405
Log2(FC) TE
log2(CPM)
B
2–cell vs 1–cell
Mutant fold change (Log2FC)
Wild–type fold change (Log2FC)
C
4–cell vs 2–cell in Zu405
Log2(FC) TE
log2(CPM)
D
4–cell vs 2–cell
Mutant fold change (Log2FC)
Wild–type fold change (Log2FC)
Density
0.0
0.1
0.2
0.3

Figure 6: Failure of translational remodeling in oma-1(zu405) reveals diverse regulatory mechanisms (A) MA plot showing changes in TE between 1-cell and 2-cell stages in *zu405* mutant embryos. The log_2 fold change in TE (y-axis) is plotted against the mean of normalized counts (x-axis). **(B)** Scatterplot comparing log_2 fold changes in TE between *zu405* mutant (y-axis) and wild-type (x-axis) for genes significantly changed in both genotypes during the 1-cell to 2-cell transition**.** Points in green indicate known OMA-1 bound transcripts. **(C)** MA plot depicting TE changes between 2-cell and 4-cell stages in *zu405* mutant embryos, with log_2 fold change in TE (y-axis) plotted against mean normalized counts (x-axis). **(D)** Scatterplot comparing log_2 fold changes in TE between *zu405* mutant (y-axis) and wild-type (x-axis) for genes significantly changed in both genotypes during the 2-cell to 4-cell transition. Points in green indicate known OMA-1 bound transcripts[34] . In all plots, the blue density overlay represents the overall distribution of genes, with intensity corresponding to the density of data points

To better understand what types of transcripts are regulated by OMA-1, we moved beyond the gene-by-gene statistical analysis (Figures 5 and 6) to a group-based approach similar to our analysis of wild-type data (Figure 3). This analysis uncovered a spectrum of translational changes among known OMA-1-bound transcript in the mutant condition, revealing four distinct response patterns (Figure 7A). We observed the enrichment of specific biological functions among the detected clusters (Figure 7B). Cluster I, which showed increased TE in the OMA-1 mutant, is enriched for transcripts associated with membrane-bound organelles. Cluster II maintained stable translation regardless of OMA-1 status and was enriched for basic cellular 'housekeeping' processes. Cluster III exhibited a minor decreased TE in OMA-1 mutants and was enriched for RNA processing and nuclear functions. Cluster III included *zif-1,* which was shown to be translationally repressed in *zu405* mutants[36], and our data also observes a similar repression (Figure S8F). Most strikingly, Cluster IV, which showed the strongest translational repression in the mutant, is enriched for developmental processes, particularly tissue development and cell fate commitment, with notable enrichment for Wnt signaling transcripts including *mom-2*, a key Wnt ligand whose translation is dramatically affected in the *oma-1(zu405)* background as confirmed by fluorescent reporters[18] (Figure S8F). The emergence of these four clusters, each with distinct temporal translational patterns and enriched biological processes, highlights the complex and varied roles of OMA-1 in regulating its target transcripts, which might be explained by OMA-1's known interactions with several other RNA-binding proteins[18,32]. Furthermore, the detection of OMA-1-bound transcripts whose translation is

504 unaffected in the mutant suggests that these transcripts may only be regulated at other stages
505 (e.g. oogenesis), or that OMA-1 binding alone is insufficient to dictate their translational
506 regulation during early embryogenesis. Together, these results reveal that OMA-1 differentially
507 regulates distinct functional groups of transcripts, with particularly strong effects on genes
508 involved in development and cell fate decisions, while having more modest or indirect effects
509 on basic cellular processes.

510

511

512

513

514

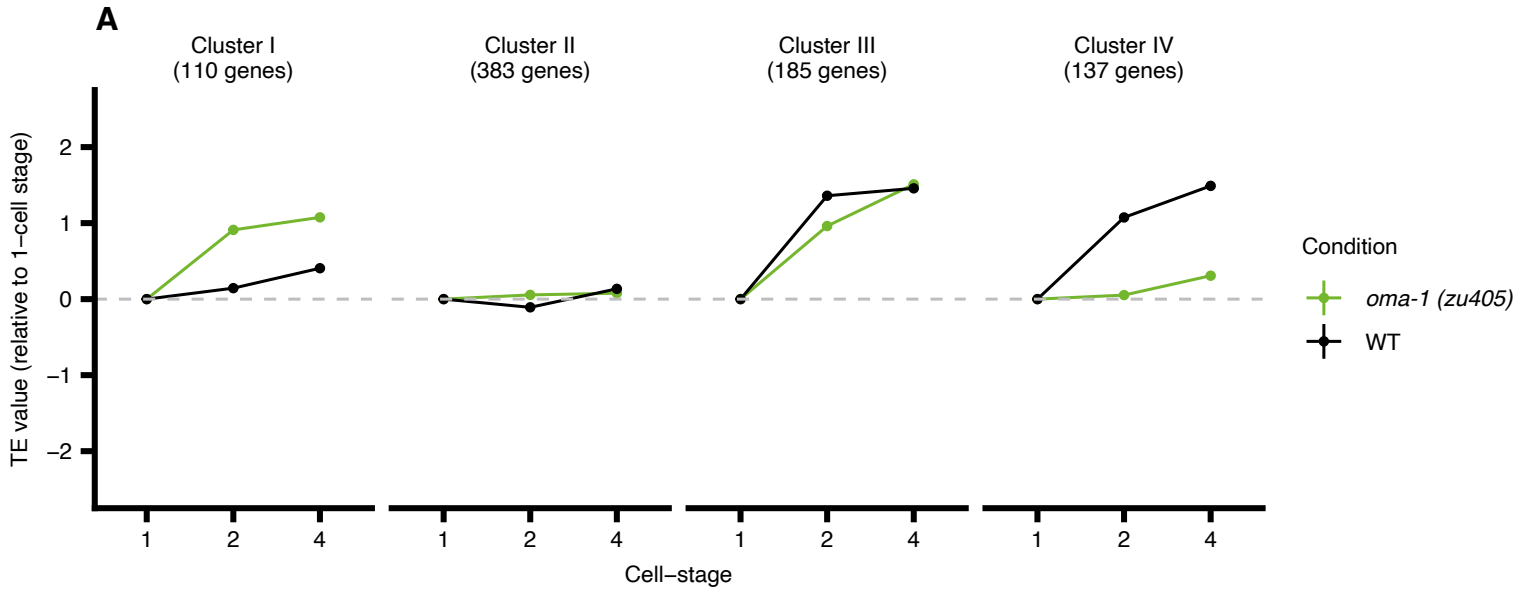
A
Cluster I
(110 genes)
Cluster II
(383 genes)
Cluster III
(185 genes)
Cluster IV
(137 genes)
TE value (relative to 1−cell stage)
2
1
0
−1
−2
1
2
4
Cell−stage
Condition
oma-1 (zu405)
WT

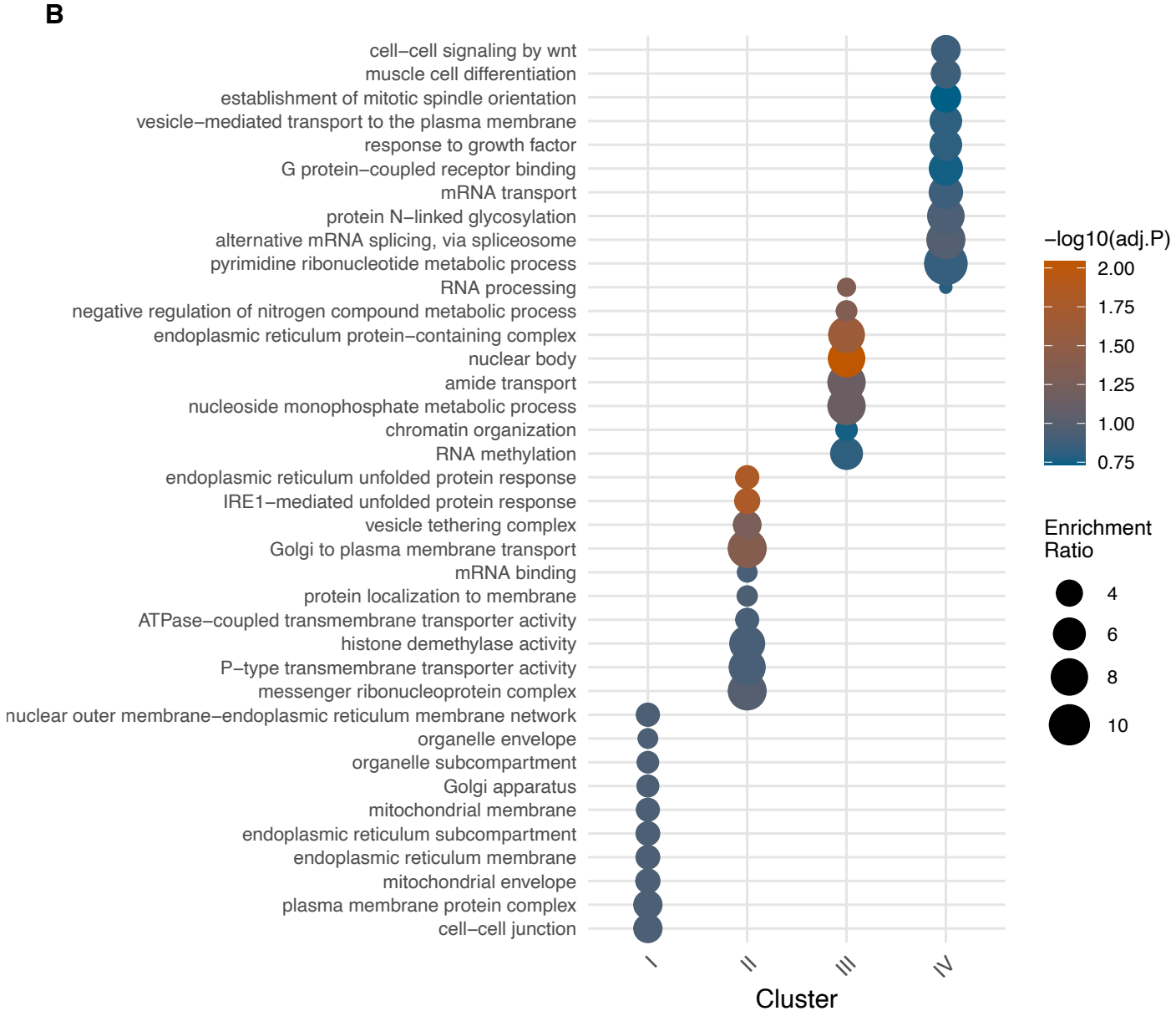
B
cell−cell signaling by wnt
muscle cell differentiation
establishment of mitotic spindle orientation
vesicle−mediated transport to the plasma membrane
response to growth factor
G protein−coupled receptor binding
mRNA transport
protein N−linked glycosylation
alternative mRNA splicing, via spliceosome
pyrimidine ribonucleotide metabolic process
RNA processing
negative regulation of nitrogen compound metabolic process
endoplasmic reticulum protein−containing complex
nuclear body
amide transport
nucleoside monophosphate metabolic process
chromatin organization
RNA methylation
endoplasmic reticulum unfolded protein response
IRE1−mediated unfolded protein response
vesicle tethering complex
Golgi to plasma membrane transport
mRNA binding
protein localization to membrane
ATPase−coupled transmembrane transporter activity
histone demethylase activity
P−type transmembrane transporter activity
messenger ribonucleoprotein complex
nuclear outer membrane−endoplasmic reticulum membrane network
organelle envelope
organelle subcompartment
Golgi apparatus
mitochondrial membrane
endoplasmic reticulum subcompartment
endoplasmic reticulum membrane
mitochondrial envelope
plasma membrane protein complex
cell−cell junction
I
II
III
IV
Cluster
−log10(adj.P)
2.00
1.75
1.50
1.25
1.00
0.75
Enrichment Ratio
4
6
8
10

Figure 7: Temporal clustering reveals diverse OMA-1-mediated translational regulation (A) Line plot showing four clusters of OMA-1-bound transcripts identified based on changes in TE. The y-axis represents TE values normalized to the 1-cell stage, and the x-axis shows developmental stages. Each line represents the mean TE trajectory for a cluster in both wild-type (black) and mutant embryos (green). Error bars represent the standard error of TE values for all genes within each cluster**. (B)** Dot plot visualizing Gene Ontology (GO) enrichment analysis for the four identified clusters. The y-axis displays enriched GO terms, while the x-axis shows the clusters. Dot size corresponds to the enrichment ratio and color intensity indicates the adjusted p-value of enrichment.

3. Discussion

Translational regulation allows precise control of protein expression in the absence of active transcription in early embryonic development across various species. Our study provides the first comprehensive, high-resolution view of translational dynamics during the initial cell divisions in *C. elegans* embryos, revealing extensive regulation of maternal mRNAs. By leveraging ribosome profiling via isotachophoresis (Ribo-ITP)[23], we overcame previous technical limitations in analyzing low-input samples from precisely staged embryos. This approach enabled us to generate high-quality ribosome footprint data from individual embryonic stages with unprecedented temporal resolution. Combined with low-input RNA-seq, we uncovered global patterns of translational control that shed light on how cell fates are specified prior to zygotic genome activation. Our findings not only extend our understanding of early embryogenesis in *C. elegans* but also provide insights into the fundamental mechanisms of post-transcriptional regulation in early animal development.

Previous studies were limited to RNA-seq and mass spectrometry analyses of oocytes, 1-cell, and 2-cell stages, and did not directly investigate translational regulation[49]. Our study demonstrates that ribosome recruitment onto mRNA is poorly correlated with mRNA abundance in the *C. elegans* early embryos. The correlation between ribosome occupancy and mRNA levels varies across species in a way that appears to correlate with the rate of embryonic development. *Drosophila* embryos (Pearson correlation = 0.348)[64] develop rapidly, with the entire embryogenesis completed in about 24 hours, while mouse embryogenesis (Spearman correlation ranging from 0.7 to 0.8)[23] takes approximately 20 days. This spectrum of

545 developmental rates and strategies extends to vertebrates as well. Zebrafish [65] and *Xenopus*
546 [66] develop faster than mammals, completing embryogenesis in 3-4 days with reduced reliance
547 on zygotic transcription[67–69]. We suspect that, like *C. elegans*, these faster-developing
548 vertebrates will depend more heavily on maternal factors and post-transcriptional regulation
549 during early embryogenesis.

550 The relationship between developmental tempo and translational regulation is further illustrated
551 by comparing *C. elegans* with the nematode *Ascaris suum*. Despite similarities in early
552 embryonic cellular organization, *A. suum* initiates zygotic genome activation at the 1-cell stage,
553 prior to pronuclear meeting[70]. Surprisingly, many of the maternal transcripts required in *C.*
554 *elegans* are zygotically produced in *A. suum*. This difference may be attributed to the vastly
555 different cell cycle durations: approximately 24 hours in *A. suum* (similar to mouse) compared
556 to 10-15 minutes in *C. elegans*. These observations suggest that organisms undergoing rapid
557 cell division may co-opt translational regulation to meet changing protein demands more
558 efficiently, with *C. elegans* representing an extreme case of rapid development and reliance on
559 post-transcriptional regulation among these model organisms.

560 During early embryonic development, maternal mRNAs are often localized to specific regions
561 of the egg or embryo, establishing developmental axes and patterns. These localized mRNAs,
562 when translated, produce proteins that initiate and maintain developmental gradients[71,72] and
563 specify cell fates[10,73]. For instance, in many organisms, mRNAs localized to the animal and
564 vegetal poles of the egg are responsible for determining the anterior-posterior and dorsal-
565 ventral axes[72]. Additionally, some localized mRNAs are crucial for germ plasm assembly and
566 germ cell development[74]. By comparing TE values for mRNAs with known subcellular
567 localization in *C. elegans*[57], we detected correlations between the localization of transcripts
568 and their respective TE. This relationship was particularly apparent for mRNAs localized to
569 specific cellular compartments, such as the cell periphery and in germline-specific

570 ribonucleoprotein complexes. Our analyses revealed that mRNAs localized to the periphery
571 were relatively translationally active, while those in P granules were translationally repressed.
572 Interestingly, prior studies suggested that the localization of some mRNAs to the cell periphery
573 may require partial translation to occur[19,57]. These findings suggest that subcellular positioning
574 of transcripts may serve as a key mechanism for fine-tuning gene expression in diverse cellular
575 processes and developmental stages across various species.

576 Our analysis further builds on recent insights[22,40,57] on the temporal relationship between
577 translational repression and P-granule association in the germline lineage. While germline-
578 localized transcripts showed consistently lower translational efficiency compared to somatic
579 transcripts, this repression preceded their enrichment in P-granules. The lack of P-granule
580 transcript enrichment at the two-cell stage, despite strong translational repression, coupled with
581 the observation that transcripts transitioning to P-granule localization were already
582 translationally repressed, suggests that initial translational control in the germline may operate
583 prior to P-granule association. These temporal observations implicate a model where
584 repression is established before transcripts become enriched in P-granules. Future studies
585 using techniques such as the SunTag [75,76] could provide direct visualization of translation
586 events in relation to P-granule localization to further validate this model.

587 P-granule transcripts can be classified into two groups based on their localization dynamics.
588 Group I transcripts maintain stable P-granule association through primordial germ cell
589 development, while Group II transcripts show transient association during early
590 embryogenesis[40]. The stronger translational repression observed in Group I compared to
591 Group II transcripts suggests that P-granules may serve as platforms for maintaining or
592 reinforcing established translational programs. This two-step model, where initial translational
593 repression might occur in the cytoplasm and is followed by P-granule-mediated maintenance
594 for Group I transcripts, provides new insights into how germline identity is established and

595 maintained during early development. The role of P-granules in maintaining translational
596 repression of Group II transcripts, however, remains to be determined.

597 Intriguingly, we observed that OMA-1-bound transcripts [34] underwent varying levels of change
598 in TE in the OMA-1 gain-of-function mutant. If these transcripts were solely controlled by OMA-
599 1, we would expect uniform changes across all targets. Instead, we observe context-dependent
600 variations, likely influenced by the cell stage and possibly by other RNA-binding proteins
601 working in concert with OMA-1[13,32,33] . Most surprisingly, while OMA-1 predominantly functions
602 as a translational repressor, a subset of transcripts showed increased TE in the gain-of-function
603 mutant (Figure 5D, orange dots above the line), suggesting OMA-1 can activate translation of
604 some transcripts. This activity could occur through direct activation of specific targets, as
605 previously demonstrated for SPN-4 and MEG-1[32], or through an indirect mechanism where
606 OMA-1 inhibits other translational repressors. Additionally, it is noteworthy that only a minority
607 of OMA-1-bound transcripts (~10%) exhibit strong translational repression at the stages we
608 analyzed, further supporting the hypothesis that effective OMA-1-mediated regulation requires
609 cooperative action with stage-specific cofactors. The clustering analysis in Figure 7A illustrates
610 these diverse regulatory behaviors. These findings emphasize the need to consider both direct
611 and indirect regulatory mechanisms and the combinatorial effects of RNA-binding proteins in
612 early embryogenesis.

613 Altogether, our work has uncovered modes of translational regulation that shape protein
614 expression during early embryogenesis. Our high-resolution temporal analysis of translational
615 dynamics provides insight into how post-transcriptional regulation directs cell fate decisions.
616 This technical advance enables systematic identification of global regulatory roles for RNA
617 binding proteins during development. The *C. elegans* model system's unique amenability to
618 both genetic manipulation and global analyses makes it ideally suited for these studies,
619 allowing us to combine our novel approaches with classical genetics in ways not possible in

other organisms. This comprehensive dataset will serve as a valuable resource for the *C. elegans* community, enabling future studies of translational control in early development and cellular differentiation.

3.1. Limitations of the Study

First, we used ribosome occupancy normalized to mRNA abundance as a proxy for translational efficiency, but note that our measurements cannot distinguish between actively translating ribosomes and stalled ribosomes on transcripts. Additionally, our approach lacks single-molecule resolution, meaning we cannot distinguish whether changes in ribosome footprint abundance represent uniform translation across all copies of a particular mRNA, or heterogeneous translation where some copies are heavily translated while others remain untranslated. This distinction may be particularly relevant in early embryos where spatial organization of mRNAs plays important developmental roles. Second, the compositional nature of any sequencing-based measurement provides only relative estimates rather than absolute measurements, which should be carefully considered when interpreting the results. Third, our RNA sequencing approach relied on poly-A selection, thereby excluding non-polyadenylated transcripts such as histones from our analysis. Fourth, our current experimental design, which examined whole embryos at the 1-cell, 2-cell, 4-cell, and 8-cell stages, lacks spatial resolution at the lineage level. The calculated translation efficiency values represent averages across different cell lineages rather than lineage-specific measurements. Future experiments could address this limitation by investigating translational regulation within specific lineages of the *C. elegans* embryo to better understand lineage-specific translational control.

4. Acknowledgments

This work was supported by National Institutes of Health grants [HD110096, GM150667] and a Welch Foundation grant [F-2027-20230405] (C.C.); and by NIH GM138443 (D.D.). We thank N. Stolpner for contributions to early project conceptualization, D. Park for experimental troubleshooting assistance, R. Tachibana for analysis validation, I. Hoskins for computational support with 3'UTR analysis, M. Modi for valuable discussions on statistical approaches and

data visualization, and Sophia Tintori and Bob Goldstein for critical reading of the manuscript. We thank Germano Cecere for sharing their translational efficiency data. We also thank members of the Cenik and Dickinson labs for helpful discussions.

5. Author contributions

Y.S., D.J.D., and C.C. conceptualized the study. Y.S. and V.G. performed ribosome profiling experiments and data analysis with guidance from C.C.. Y.S. analyzed P-granule localization data. C.H. performed imaging experiments and analysis under supervision from D.J.D.. Y.S. performed bioinformatics analysis with input from C.C.. Y.S. wrote the manuscript with input from all authors. Y.S. prepared the figures with suggestions from V.G., D.J.D., and C.C.. D.J.D. and C.C. supervised the project.

6. Declaration of interests

The authors declare that they have no competing interests related to this work.

7. Declaration of generative AI and AI-assisted technologies

During the preparation of this work, we used Claude (Anthropic) for three purposes: (1) to improve grammar and clarity of scientific writing, (2) to generate code for data visualization and statistical analysis, which was subsequently reviewed and modified. All AI-generated content was carefully reviewed, edited, and validated by the authors. The authors take full responsibility for the accuracy and completeness of the published manuscript.

8. Accession number

The accession number for all libraries reported in this paper is NCBI GEO: GSE281412. Original image data will be deposited in the Texas Data Repository (https://dataverse.tdl.org), with DOI: https://doi.org/10.18738/T8/EFJNGZ.

9. Code availability

The code used in the study is available at https://github.com/yss322/Low-input-ribosome-profiling-of-Celegans-embryogenesis

10. Supplemental information titles and legends

Document S1: Figures S1–S7 and Table S1-S5 description

Table S1: Count Data for RNA Sequencing and Ribosome Profiling

Table S2: GO annotations Gene Ontology Enrichment Analysis Results for WT

Table S3: Fisher's Exact Test Analysis of P-Granule and Germline-Enriched Gene Overlap

Table S4: Linear Regression Analysis of RNA-Binding Protein Effects on Translation Efficiency

679 **Table S5:** Gene Ontology Enrichment Analysis of OMA-1-Regulated Transcript Clusters

680

681 ## 11. Supplementary Figures

682

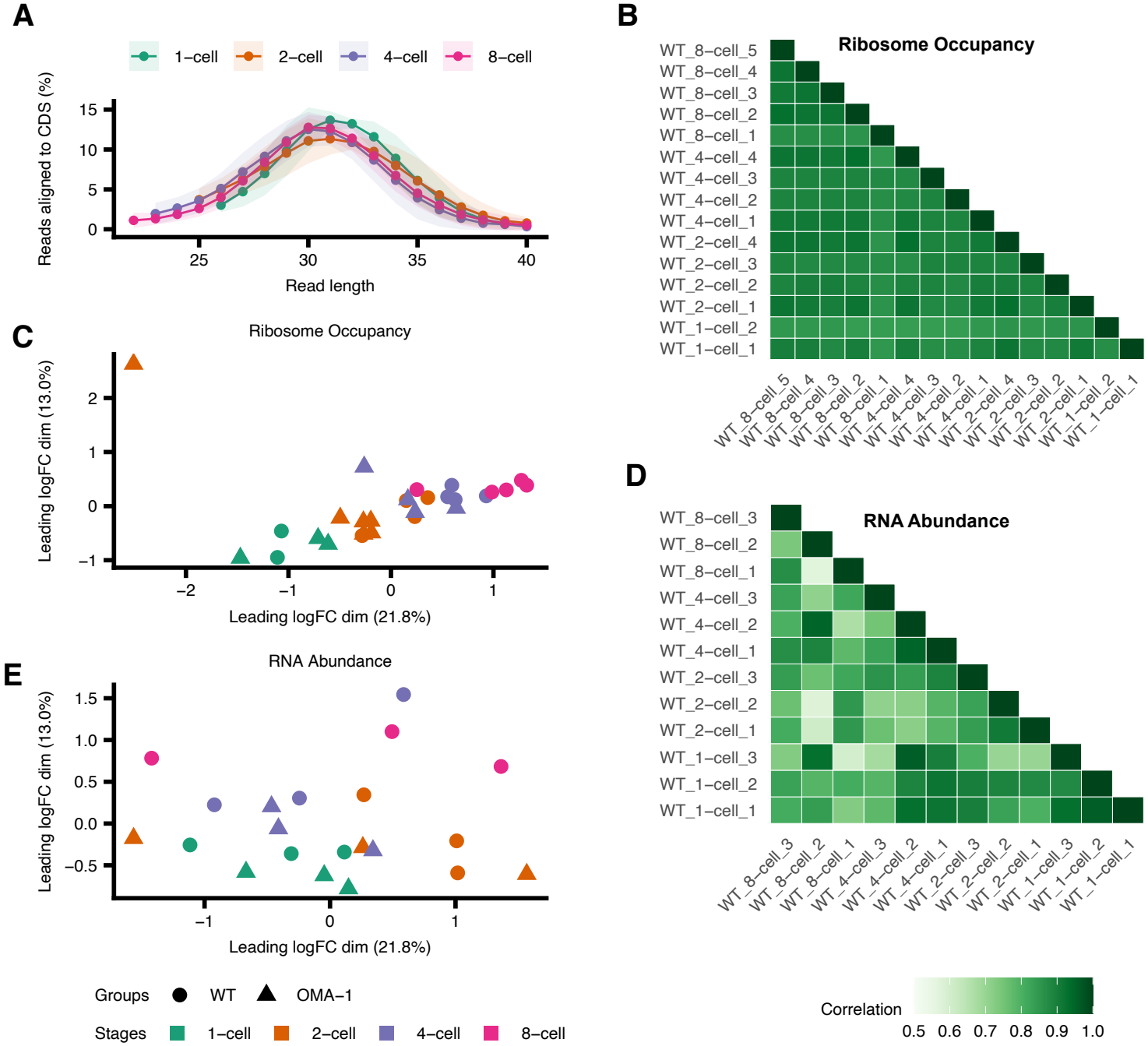
A
1–cell
2–cell
4–cell
8–cell
Reads aligned to CDS (%)
Read length
B
Ribosome Occupancy
WT_8–cell_5
WT_8–cell_4
WT_8–cell_3
WT_8–cell_2
WT_8–cell_1
WT_4–cell_4
WT_4–cell_3
WT_4–cell_2
WT_4–cell_1
WT_2–cell_4
WT_2–cell_3
WT_2–cell_2
WT_2–cell_1
WT_1–cell_2
WT_1–cell_1
C
Ribosome Occupancy
Leading logFC dim (13.0%)
Leading logFC dim (21.8%)
D
RNA Abundance
WT_8–cell_3
WT_8–cell_2
WT_8–cell_1
WT_4–cell_3
WT_4–cell_2
WT_4–cell_1
WT_2–cell_3
WT_2–cell_2
WT_2–cell_1
WT_1–cell_3
WT_1–cell_2
WT_1–cell_1
E
RNA Abundance
Leading logFC dim (13.0%)
Leading logFC dim (21.8%)
Groups
WT
OMA–1
Stages
1–cell
2–cell
4–cell
8–cell
Correlation
0.5 0.6 0.7 0.8 0.9 1.0

683 ***11.1. Figure S1:***

684 **(A)** Distribution of ribosome profiling read lengths across developmental stages, with shaded
685 areas indicating standard deviation between biological replicates**. (B)** Correlation matrix of
686 ribosome occupancy, where darker colors indicate stronger correlations. **(C)** Multidimensional
687 scaling analysis of Ribo-seq. Axes represent arbitrary units. **(D)** Correlation matrix of RNA
688 abundance between replicates, where darker colors indicate stronger correlations. **(E)** RNA-
689 seq replicates, with shapes denoting WT versus OMA-1 mutants and colors indicating cell
690 stages. Axes represent arbitrary units.

691

692

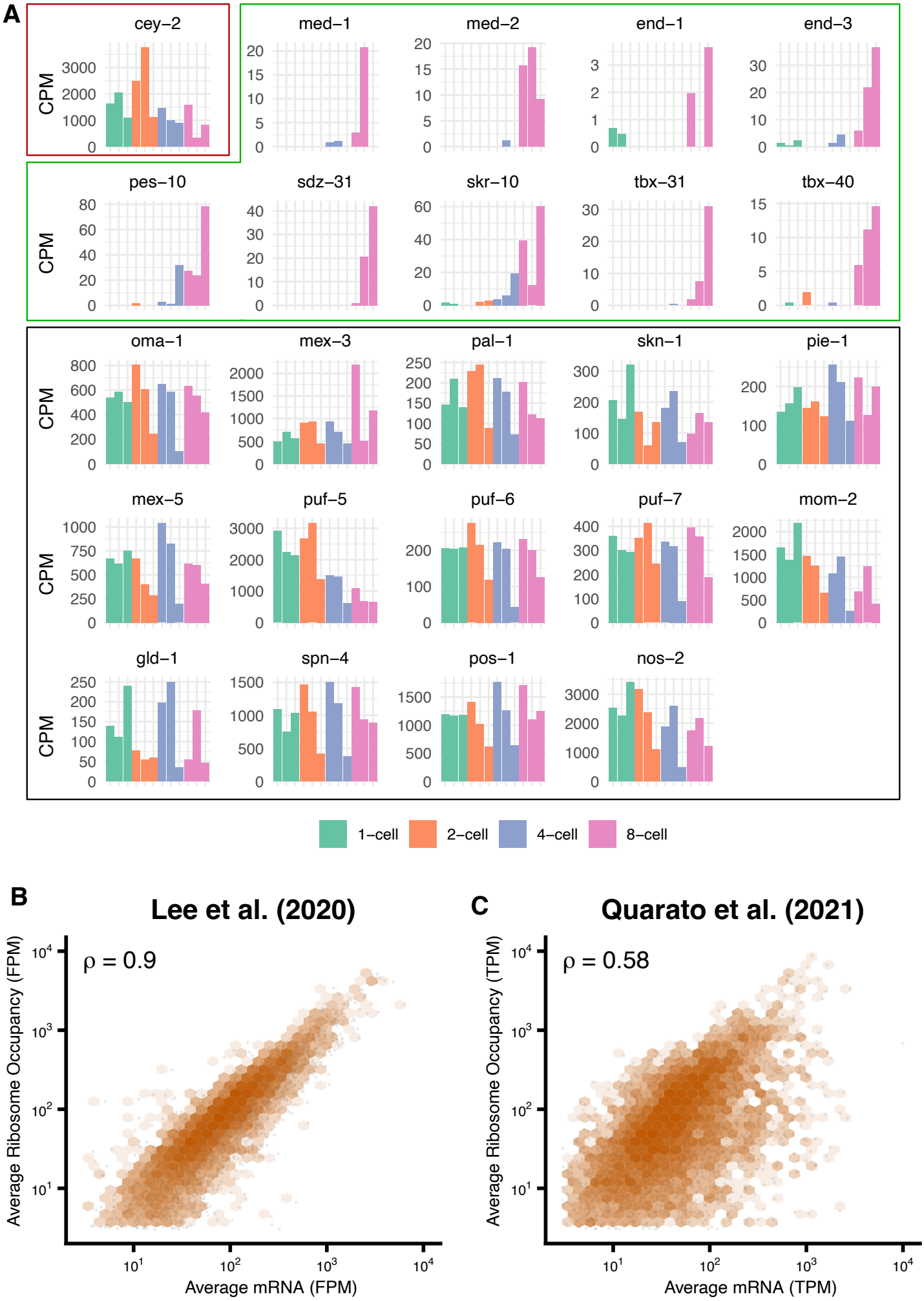
A
cey−2
med−1
med−2
end−1
end−3
pes−10
sdz−31
skr−10
tbx−31
tbx−40
oma−1
mex−3
pal−1
skn−1
pie−1
mex−5
puf−5
puf−6
puf−7
mom−2
gld−1
spn−4
pos−1
nos−2
CPM
1−cell
2−cell
4−cell
8−cell
B
Lee et al. (2020)
ρ = 0.9
Average Ribosome Occupancy (FPM)
Average mRNA (FPM)
C
Quarato et al. (2021)
ρ = 0.58
Average Ribosome Occupancy (TPM)
Average mRNA (TPM)

693 ***11.2. Figure S2:***

694 (A) Expression patterns from RNA-seq of marker genes, highlighting cey-2 in red box showing
695 progressive degradation throughout embryogenesis, while genes predominantly expressed at
696 the 8-cell stage are in green box. Other previously identified maternally deposited mRNA are
697 shown in the black box. Each bar in the plot of the same color represents a replicate.
698 Relationship between mRNA abundance and ribosome occupancy from (B) Lee et al. (C)
699 Quarato et al. (2021). The plot shows average mRNA levels versus average ribosome
700 occupancy on log10 scales. Gray dots represent individual genes with hexagonal binning
701 (orange) indicating data density. The Spearman correlation coefficient (rho) quantifies the
702 relationship strength

703

704

705

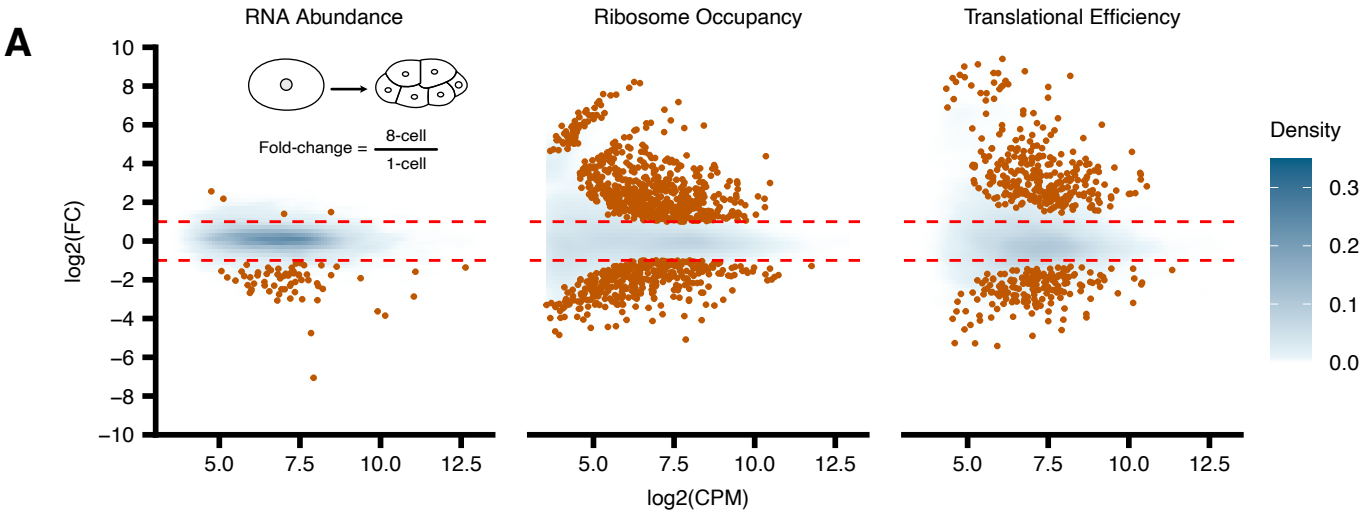
A
RNA Abundance
Ribosome Occupancy
Translational Efficiency
Fold-change = 8-cell / 1-cell
log2(FC)
log2(CPM)
Density
0.3
0.2
0.1
0.0

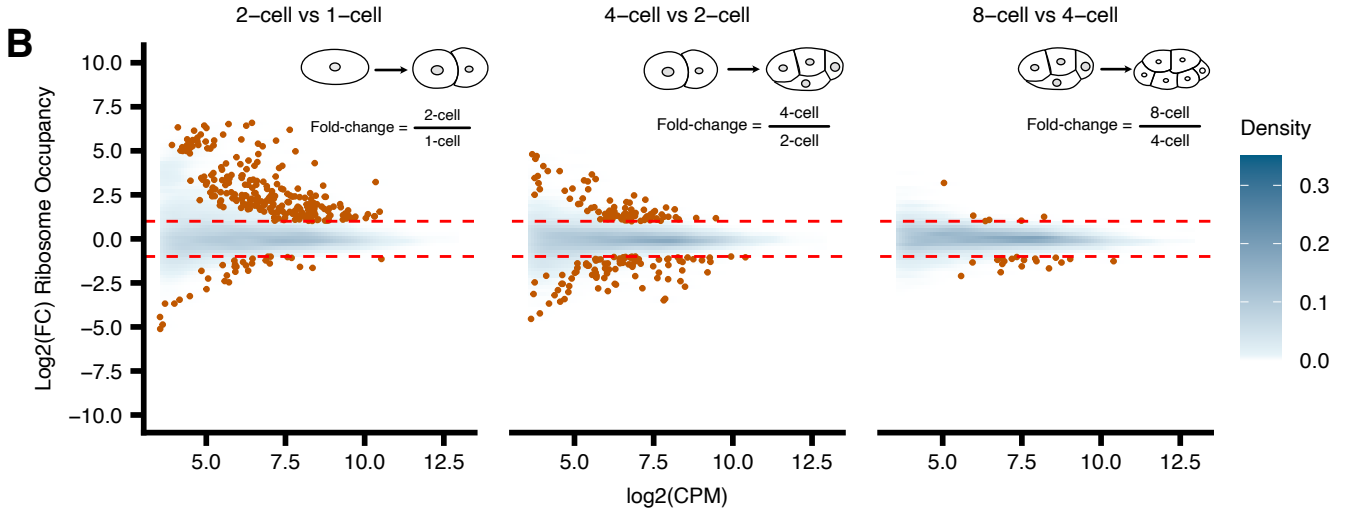
B
2–cell vs 1–cell
4–cell vs 2–cell
8–cell vs 4–cell
Fold-change = 2-cell / 1-cell
Fold-change = 4-cell / 2-cell
Fold-change = 8-cell / 4-cell
Log2(FC) Ribosome Occupancy
log2(CPM)
Density
0.3
0.2
0.1
0.0

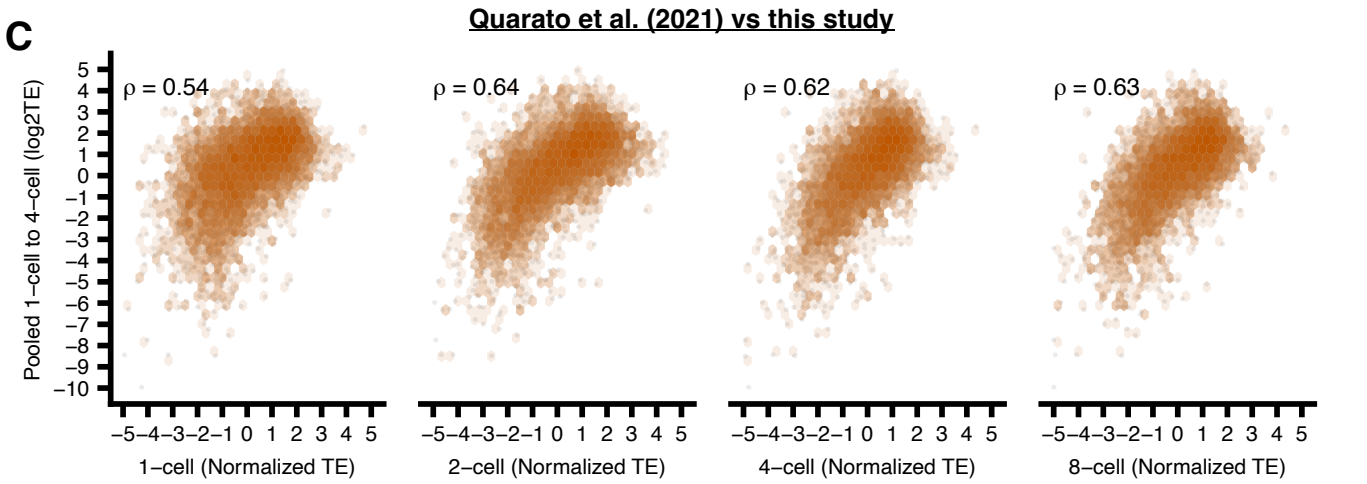
C
Quarato et al. (2021) vs this study
ρ = 0.54
ρ = 0.64
ρ = 0.62
ρ = 0.63
Pooled 1–cell to 4–cell (log2TE)
1–cell (Normalized TE)
2–cell (Normalized TE)
4–cell (Normalized TE)
8–cell (Normalized TE)

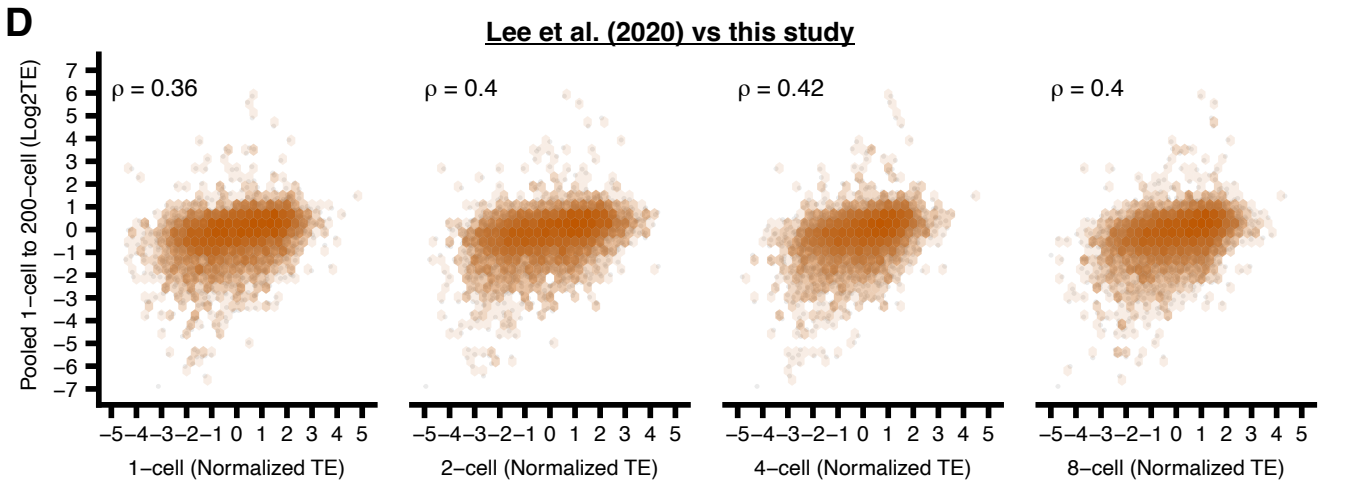
D
Lee et al. (2020) vs this study
ρ = 0.36
ρ = 0.4
ρ = 0.42
ρ = 0.4
Pooled 1–cell to 200–cell (Log2TE)
1–cell (Normalized TE)
2–cell (Normalized TE)
4–cell (Normalized TE)
8–cell (Normalized TE)

706 ***11.3. Figure S3:***

707

708 **(A)** Mean difference plots comparing RNA abundance, ribosome occupancy, and translational
709 efficiency between 8-cell and 1-cell stage wild-type embryos. X-axis shows expression level
710 (log2CPM), Y-axis shows $\log_2$ fold change. Mean difference plots comparing gene expression
711 between sequential *C. elegans* embryonic stages **(B)**1-cell to 2-cell, 2-cell to 4-cell, and 4-cell
712 to 8-cell. The log2 fold change in ribosome occupancy (y-axis) is plotted against the mean of
713 normalized counts (x-axis). Blue density plot represents the overall distribution of genes with
714 the intensity corresponds to the density of points. The orange points indicate transcripts with
715 significant expression changes (FDR < 0.2 and $\log_2$FC >1 or < -1). Blue density indicates
716 concentration of data points. Orange points highlight significant changes (|$\log_2$FC| > 1, FDR <
717 0.05). Red dashed lines indicate ±1 $\log_2$FC thresholds. Correlations between stage-specific
718 and pooled embryonic translational efficiencies. **(C)** Comparison of normalized TE at the same
719 developmental stages with pooled 1-cell to 4-cell TE data from Quarato et al. (2021) (y-axes).
720 **(D)** Comparison of normalized translational efficiency (TE) at 1-cell, 2-cell, 4-cell, and 8-cell
721 stages (x-axes) with pooled 1-cell to 200-cell TE data from Lee et al. (2020) (y-axes). Orange
722 hexagonal binning shows data density with Spearman correlation coefficients (rho) indicating
723 relationship strength.

724

725

726

727

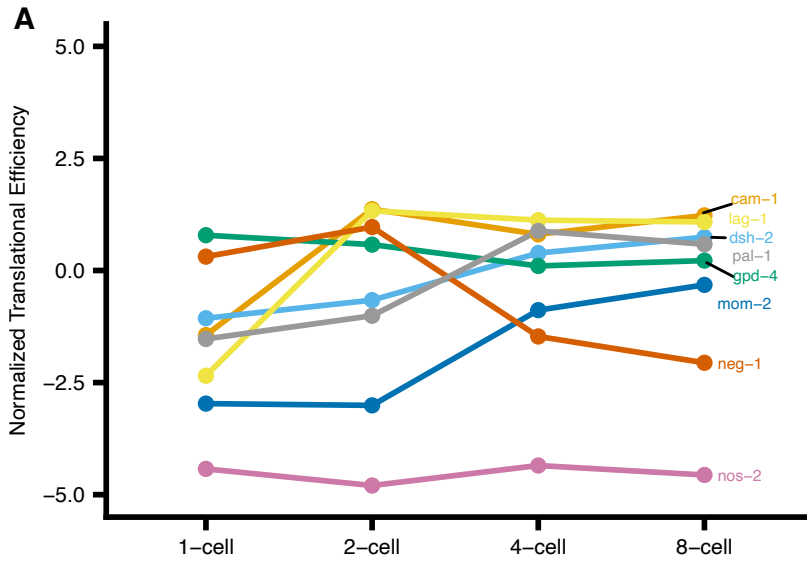
A
Normalized Translational Efficiency
5.0
2.5
0.0
−2.5
−5.0
1−cell
2−cell
4−cell
8−cell
cam−1
lag−1
dsh−2
pal−1
gpd−4
mom−2
neg−1
nos−2

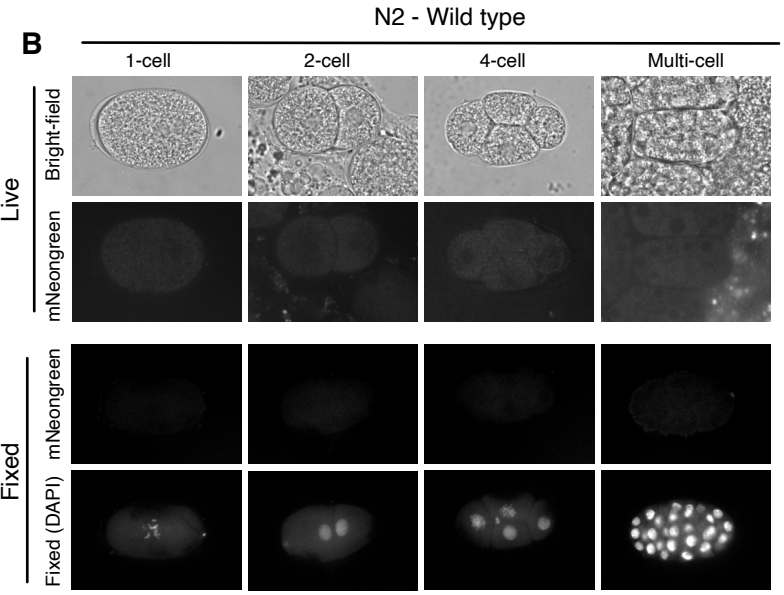
B
N2 - Wild type
1-cell
2-cell
4-cell
Multi-cell
Live
Bright-field
mNeongreen
Fixed
mNeongreen
Fixed (DAPI)

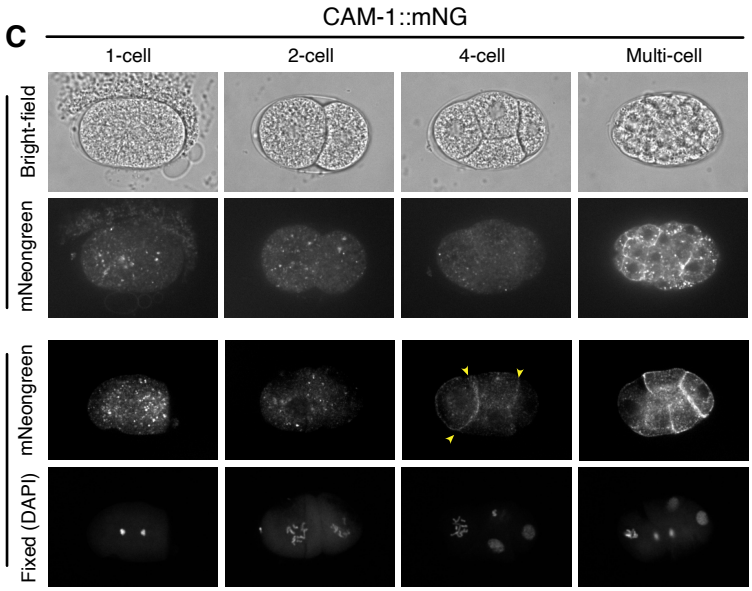
C
CAM-1::mNG
1-cell
2-cell
4-cell
Multi-cell
Bright-field
mNeongreen
mNeongreen
Fixed (DAPI)

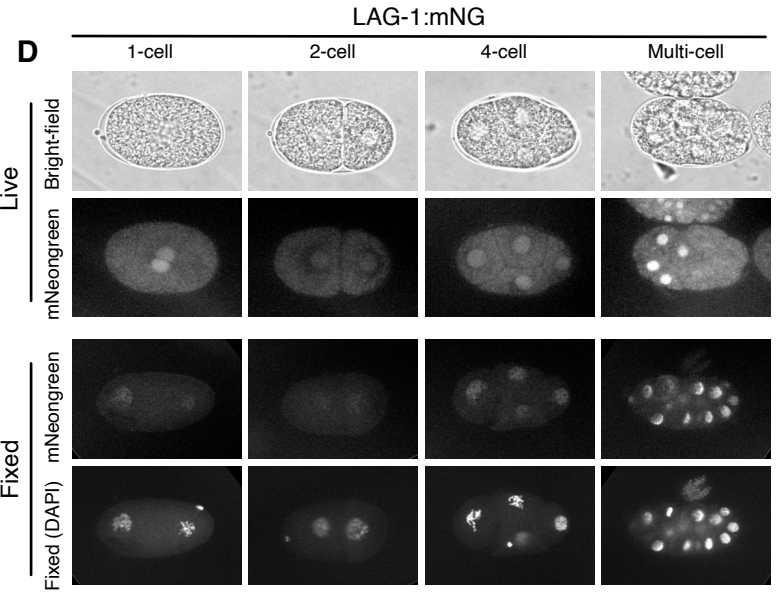
D
LAG-1:mNG
1-cell
2-cell
4-cell
Multi-cell
Live
Bright-field
mNeongreen
Fixed
mNeongreen
Fixed (DAPI)

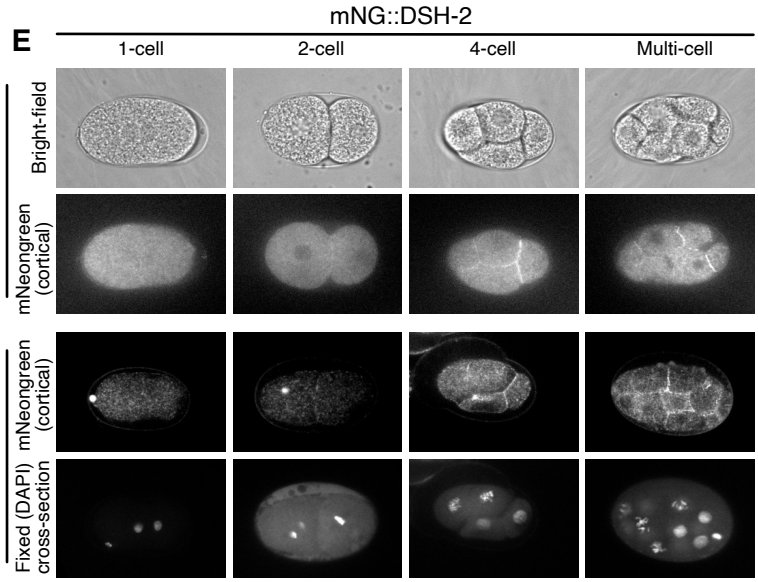
E
mNG::DSH-2
1-cell
2-cell
4-cell
Multi-cell
Bright-field
mNeongreen (cortical)
mNeongreen (cortical)
Fixed (DAPI) cross-section

728 ***11.4. Figure S4:***

729 **(A)** Normalized TE profiles of previously identified (PAL-1, MOM-2, NEG-1, NOS-2) and newly
730 identified (CAM-1, LAG-1 and DSH-1) translationally regulated transcripts compared to the
731 housekeeping gene GPD-4. **(B-E)** Localization of newly identified proteins during early
732 embryonic development. **(B)** N2 control, **(C)** CAM-1::mNG, **(D)** LAG-1::mNG, and **(E)** DSH-
733 1::mNG embryos imaged at 1-cell, 2-cell, 4-cell, and multicellular stages. For each genotype:
734 brightfield (top row), live mNG fluorescence (middle row), and fixed samples showing mNG
735 signal with DAPI counterstain (bottom row). Arrowheads indicate cell-cell contact localization
736 of fluorescently tagged proteins in CAM-1::mNG.

737

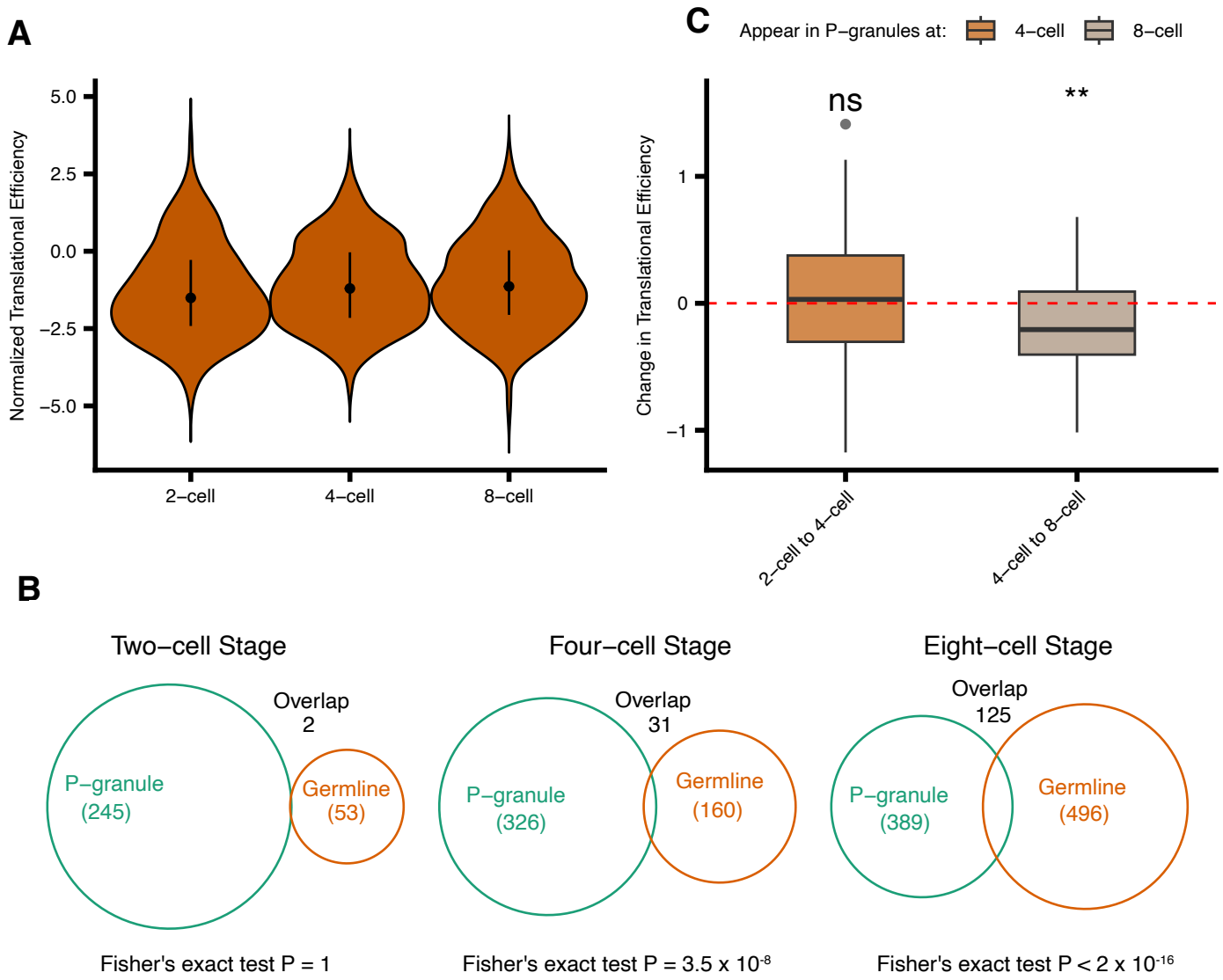
A
Normalized Translational Efficiency
5.0
2.5
0.0
−2.5
−5.0
2−cell
4−cell
8−cell
C
Appear in P−granules at:
4−cell
8−cell
Change in Translational Efficiency
ns
**
1
0
−1
2−cell to 4−cell
4−cell to 8−cell
B
Two−cell Stage
Overlap
2
P−granule
(245)
Germline
(53)
Fisher's exact test P = 1
Four−cell Stage
Overlap
31
P−granule
(326)
Germline
(160)
Fisher's exact test P = 3.5 x 10-8
Eight−cell Stage
Overlap
125
P−granule
(389)
Germline
(496)
Fisher's exact test P < 2 x 10-16

11.5. Figure S5:

(A) Translational efficiency of P-granule localized transcripts across developmental stages. Violin plots show distribution of TE values for P-granule transcripts at 2-cell (n=245), 4-cell (n=326), and 8-cell (n=389) stages, with median and quartiles indicated. **(B)** The overlap between P-granule-associated genes and genes expressed at specific developmental stages in *C. elegans* early embryogenesis. The Venn diagrams illustrate three developmental timepoints: two-cell, four-cell, and eight-cell stage. **(C)** Changes in translational efficiency of transcripts as they transition into P-granules. Box plots show TE changes for transcripts first appearing in P-granules at 4-cell (orange, n=81) and 8-cell stages (brown, n=43). Red dashed line indicates no change in TE. Asterisks denote significant differences from zero (***$p < 0.001$, Wilcoxon test).

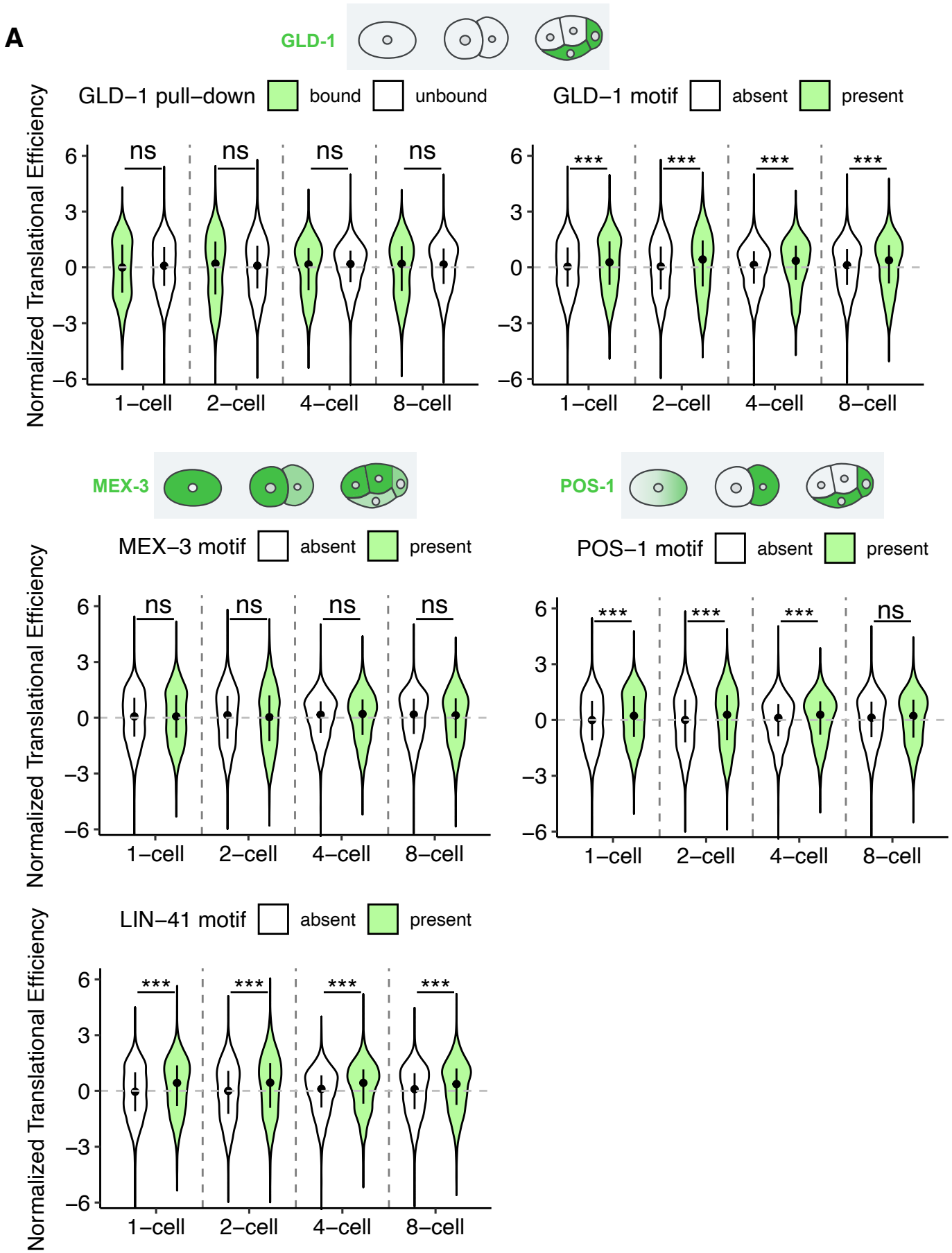
A
GLD-1
GLD−1 pull−down
bound
unbound
GLD−1 motif
absent
present
Normalized Translational Efficiency
ns
***
1−cell
2−cell
4−cell
8−cell
MEX-3
MEX−3 motif
POS-1
POS−1 motif
LIN−41 motif

751 ***11.6. Figure S6:***

752 Violin plots showing the distribution of normalized translational efficiency for transcripts across
753 early *C. elegans* embryonic stages (1-cell, 2-cell, 4-cell, and 8-cell). Comparisons are shown
754 between: **(A)** GLD-1-bound versus unbound transcripts from RNA-immunoprecipitation data,
755 and transcripts with present versus absent motifs for **(B)** POS-1, **(C)** MEX-3, **(D)** GLD-1, and
756 **(E)** LIN-41. Green violins represent bound/motif-present transcripts, while white violins indicate
757 unbound/motif-absent transcripts. Plot width indicates probability density of translational
758 efficiency values(***$p < 0.001$, Wilcoxon test). Illustrations indicate known localization of
759 proteins during early embryogenesis

760

761

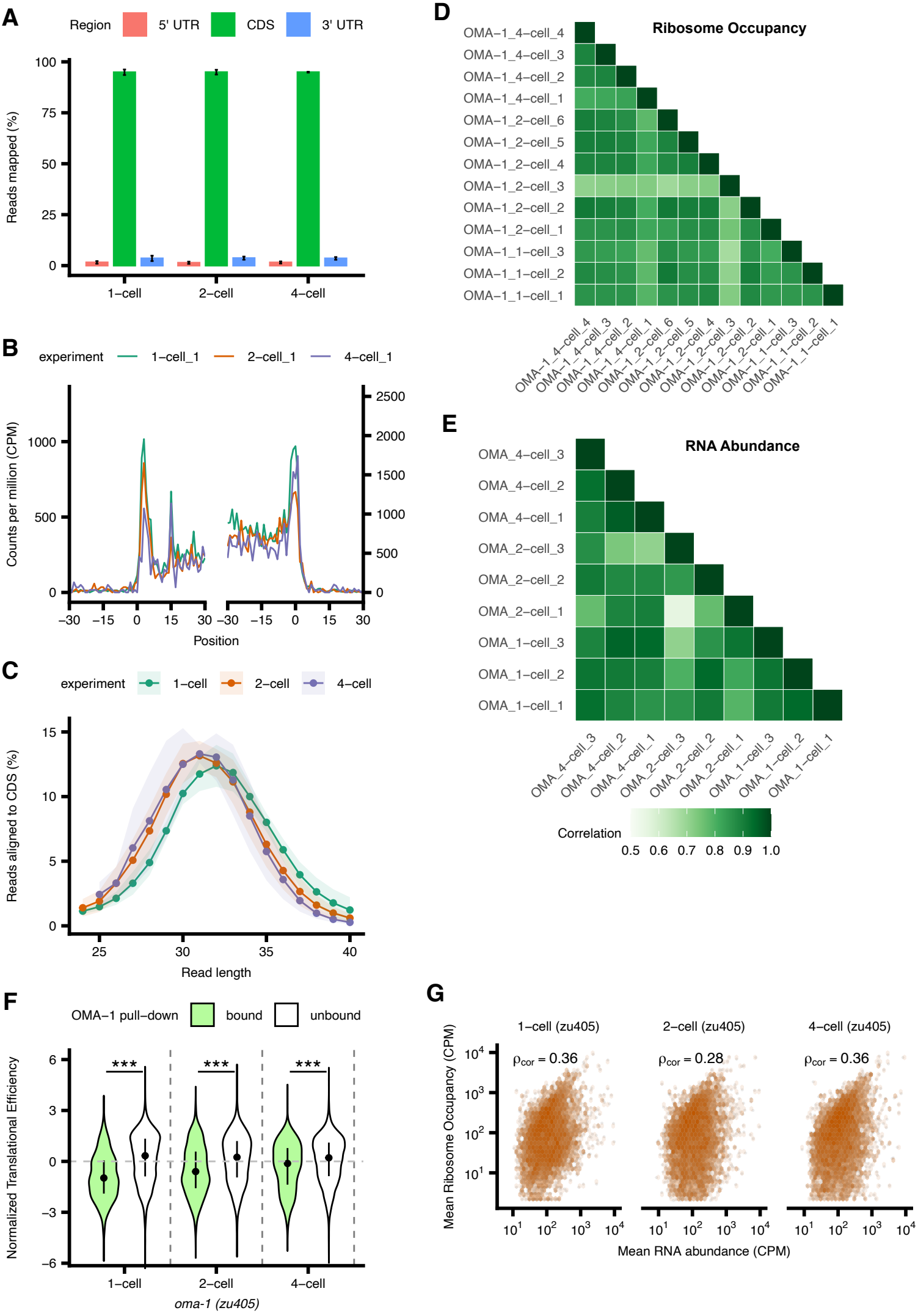
A
Region
5' UTR
CDS
3' UTR
Reads mapped (%)
100
75
50
25
0
1–cell
2–cell
4–cell
B
experiment
1–cell_1
2–cell_1
4–cell_1
Counts per million (CPM)
1000
500
0
2500
2000
1500
1000
500
0
–30
–15
0
15
30
Position
C
experiment
1–cell
2–cell
4–cell
Reads aligned to CDS (%)
15
10
5
0
25
30
35
40
Read length
D
Ribosome Occupancy
OMA–1_4–cell_4
OMA–1_4–cell_3
OMA–1_4–cell_2
OMA–1_4–cell_1
OMA–1_2–cell_6
OMA–1_2–cell_5
OMA–1_2–cell_4
OMA–1_2–cell_3
OMA–1_2–cell_2
OMA–1_2–cell_1
OMA–1_1–cell_3
OMA–1_1–cell_2
OMA–1_1–cell_1
E
RNA Abundance
OMA_4–cell_3
OMA_4–cell_2
OMA_4–cell_1
OMA_2–cell_3
OMA_2–cell_2
OMA_2–cell_1
OMA_1–cell_3
OMA_1–cell_2
OMA_1–cell_1
Correlation
0.5
0.6
0.7
0.8
0.9
1.0
F
OMA–1 pull–down
bound
unbound
Normalized Translational Efficiency
6
3
0
–3
–6
***
1–cell
2–cell
4–cell
oma-1 (zu405)
G
1–cell (zu405)
2–cell (zu405)
4–cell (zu405)
ρ_{cor} = 0.36
ρ_{cor} = 0.28
ρ_{cor} = 0.36
Mean Ribosome Occupancy (CPM)
10^4
10^3
10^2
10^1
Mean RNA abundance (CPM)

762 ***11.7. Figure S7:***

763 **(A)**The allocation of ribosome profiling reads across genomic features (CDS, 5' UTR, 3' UTR)
764 is presented for each stage in *zu405* mutants. **(B)** Ribosome occupancy around the translation
765 start and stop sites in a representative 1-cell, 2-cell and 4-cell *zu405* staged embryo.
766 Translation start (or stop) sites are denoted by the position 0. Aggregated read counts (*y* axis)
767 relative to the start (or stop) sites are plotted after A-site correction **(C)** Distribution of ribosome
768 profiling read lengths across developmental stages, with shaded areas indicating standard
769 deviation between biological replicates**. (D)** Correlation matrix of ribosome occupancy and **(E)**
770 RNA abundance between replicates, where darker colors indicate stronger correlations. **(F)**
771 Violin plots in illustrate the distribution of normalized translational efficiency for OMA-1-bound
772 (green) and unbound (white) transcripts across three early *zu405* embryonic stages (1-cell, 2-
773 cell and 4-cell) identified from previous RNA-immunoprecipitation data. The width of each violin
774 represents the probability density of efficiency values(***$p < 0.001$, Wilcoxon test). **(G)** Pairwise
775 correlation between ribosome occupancy and RNA abundance at the three stages of early
776 *zu405* embryo development is presented. The mean cpm of ribosome occupancy is plot against
777 the mean cpm of RNA abundance at each stage. Rho (cor) is the corrected spearman
778 correlation based on the reliability r (RNA) and r (Ribo) which are the replicate-to-replicate
779 correlation (methods).

780

781

782

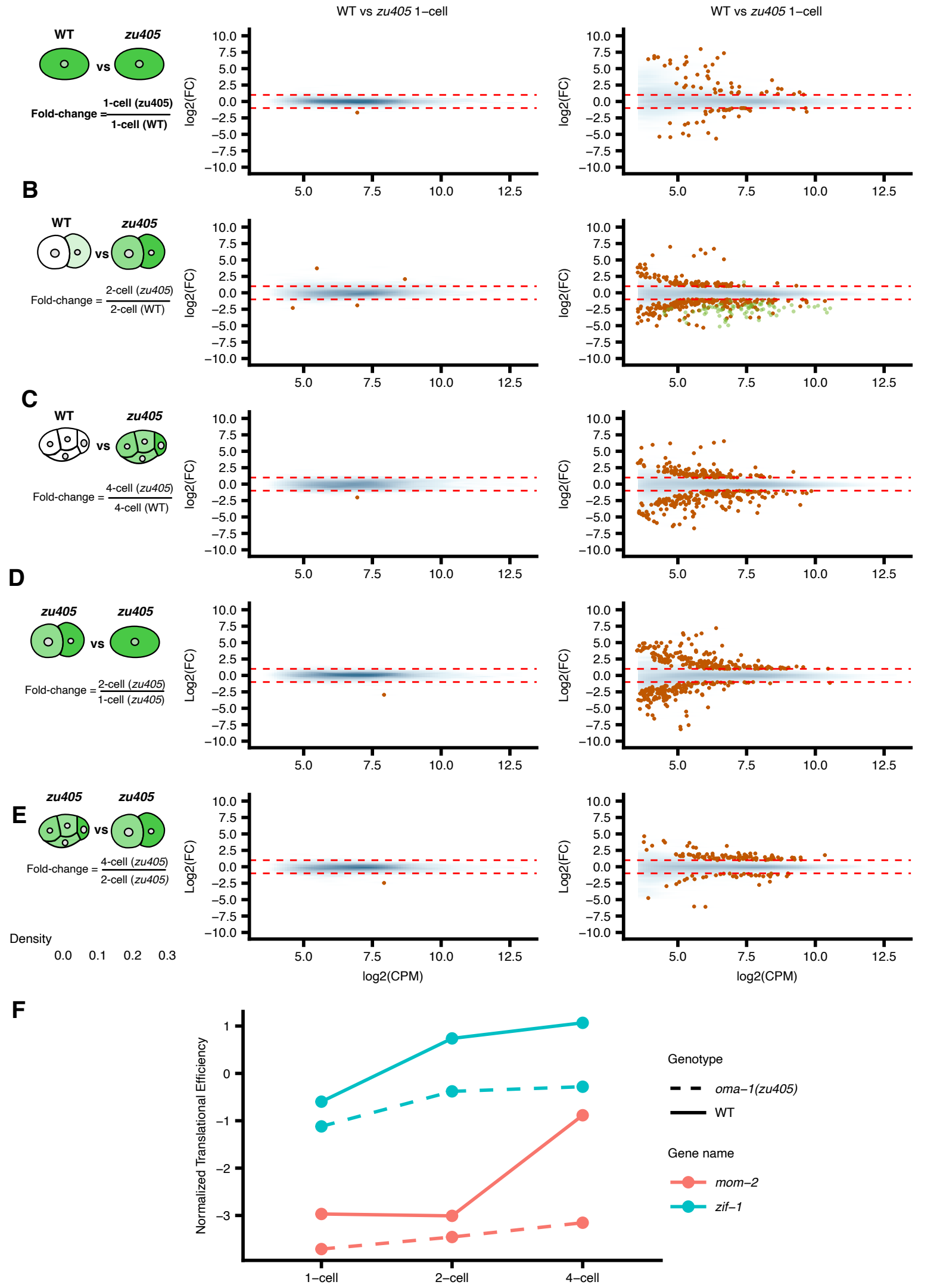
WT vs zu405 1−cell
WT vs zu405 1−cell
WT
zu405
vs
Fold-change = 1-cell (zu405) / 1-cell (WT)
log2(FC)
B
WT
zu405
vs
Fold-change = 2-cell (zu405) / 2-cell (WT)
log2(FC)
C
WT
zu405
vs
Fold-change = 4-cell (zu405) / 4-cell (WT)
log2(FC)
D
zu405
zu405
vs
Fold-change = 2-cell (zu405) / 1-cell (zu405)
Log2(FC)
E
zu405
zu405
vs
Fold-change = 4-cell (zu405) / 2-cell (zu405)
Log2(FC)
Density
0.0 0.1 0.2 0.3
log2(CPM)
log2(CPM)
F
Normalized Translational Efficiency
1−cell
2−cell
4−cell
Genotype
oma−1(zu405)
WT
Gene name
mom−2
zif−1

783 ***11.8. Figure S8:***

784 Mean difference plots comparing gene expression between *zu405* mutant and wild-type
785 embryos. **(A-C)** Comparisons between *zu405* and wild-type at 1-cell, 2-cell, and 4-cell stages,
786 respectively. **(D-E)** Stage-to-stage comparisons within zu405 embryos from 1-cell to 2-cell
787 and 2-cell to 4-cell. For all plots, $\log_2$ fold changes in RNA abundance and translational
788 efficiency (y-axis) are plotted against mean normalized counts (x-axis). Blue density shading
789 indicates the distribution of all genes, with darker shading representing higher point density.
790 Orange points highlight significantly differentially expressed genes (FDR < 0.2 and $|\log_2 FC| >$
791 1). **(F)** Developmental dynamics of translational efficiency for mom-2 and zif-1 in wild-type
792 and oma-1 mutant embryos. The plot compares normalized translational efficiency (TE) of
793 mom-2 and zif-1 genes across early embryonic stages (1-cell, 2-cell, and 4-cell) in both wild-
794 type (WT, solid lines) and oma-1(zu405) mutant (dashed lines) backgrounds.

795

796

13. STAR Methods

Key resources table

REAGENT or RESOURCE	SOURCE	IDENTIFIER
Chemicals, peptides, and recombinant proteins		
Cycloheximide	Sigma	Cat#C4859-1ML
T4 Polynucleotide Kinase	New England Biolabs	Cat#M0201L
Sodium Hypochlorite	Sigma	Catalog Number: 239305
Inulin	Thermo	Catalog Number: A18425.18
PVP Powder	Thermo	Catalog Number: 227545000
BME Vitamins	Sigma	Catalog Number: B6891
Chemically Defined Lipid Concentrate	Gibco	Catalog Number: 11905031
Penicillin-Streptomycin	Sigma	Catalog Number: P4333
Schneider's Drosophila Medium	Gibco	Catalog Number: 21720024
Fetal Bovine Serum (FBS)	Gibco	Catalog Number: A3840001
Critical commercial assays		
D-Plex Small RNA-seq Kit	Diagenode	Cat#C05030001
NEBNext Single Cell/Low Input RNA Library Prep Kit for Illumina	New England Biolabs	Cat#E6420S/L
Deposited data		
Raw and analyzed data	This Paper	GEO: GSE281412
C. elegans reference files	Liu et al[44]	https://github.com/RiboBase/reference_caenorhabditis-elegans
Study code and analysis	This Paper	https://github.com/yss322/Low-input-ribosome-profiling-of-Celegans-embryogenesis
Raw image data	This Paper	Texas Data Repository https://doi.org/10.18738/T8/EFJNGZ
Experimental models: Organisms/strains		
C. elegans: Wild type N2	Caenorhabditis Genetics Center	N2
C. elegans OMA-1 mutant strain	Lin R. et al[31]	TX20 Genotype: *oma-1(zu405)* IV.
C. elegans CAM-1::mNG::3xFLAG strain	Heppert et al[56]	LP530 Genotype: *cam-1(cp243[cam-1::mNG-C1^3xFlag]*) II.

C. elegans DSH-2::mNG::3xFLAG strain	Heppert et al[56]	LP228 dsh-2(cp51[mNeonGreen::dsh-2]) II
C. elegans LAG-1::mNG	This study	UTX259 lag-1(dev208([lag-1::mNeonGreen]) IV
Software and algorithms		
RiboFlow	Ozadam et al[77]	https://github.com/ribosomeprofiling/riboflow
UMI-tools	Smith et al[78]	https://umi-tools.readthedocs.io/en/latest/reference/extract.html
Bowtie2	Langmead and Salzberg[79]	http://bowtie-bio.sourceforge.net/bowtie2/index.shtml
Cutadapt	Marcel Martin[80]	https://cutadapt.readthedocs.io/en/stable/#
ComBat-seq	Zhang et al[81]	https://github.com/zhangyuqing/ComBat-seq
edgeR	Robinson et al[82]	https://bioconductor.org/packages/release/bioc/html/edgeR.html
clusterProfiler	Yu et al[83]	https://guangchuangyu.github.io/software/clusterProfiler/
Micro-Manager	Edelstein et al[84]	https://micro-manager.org/

13.1. Experimental model details

C. elegans maintenance

C. elegans strains were maintained on standard NGM plates and fed OP50 E. coli. The N2 (wild type) and LP530 strains were maintained at 20°C and the TX20 strain was maintained at 15°C.

13.2. Method Details

Embryo collection

For wild-type strains, embryos were collected as follows: Microscope slides were prepared by placing five Eppendorf tube stickers in a row and applying Sigmacote to the surrounding area. After drying under a fume hood for 5-10 minutes, the slides were washed with water and the stickers removed, creating wells. For embryo collection, approximately 20 worms were placed in 100 µL of egg buffer and dissected. 10 µL of bleach was added, and the solution was pipetted for 10 seconds. Eggs were selected and washed five times through 100 µL of SGM in the wells created on the treated slides (taking ~ 2 mins). After reaching the desired stage, eggs were washed five times in water, then in water with 100 µg/ml cycloheximide (CHX). During the final wash, embryos were inspected using a microscope, and those not at the correct stage were segregated. The

correctly staged embryos were transferred to a PCR tube, flash-frozen in liquid nitrogen, and then kept on a metal rack placed on dry ice. More embryos were added to the same PCR tube on dry ice, with the tube being flash-frozen in liquid nitrogen each time new embryos were added. This process was repeated until 9 embryos were collected in a single PCR tube for each stage.

For TX20 *C. elegans* strains, L4/young adult worms were incubated overnight at 20°C prior to collection. Following this incubation, the same collection process as described for wild-type strains was conducted.

Embryos were staged as follows: 1-cell stage embryos were collected prior to nuclear envelope breakdown. For 2-cell stage, 1-cell embryos were collected and monitored until they divided. Once the first embryo reached the 2-cell stage, a timer was started, and collection of 2-cell embryos continued for 5 minutes. Similarly, for the 4-cell stage, 2-cell embryos were collected and monitored until they divided. When the first embryo reached the 4-cell stage, a timer was started, and collection of 4-cell embryos continued for 5 minutes. For the 8-cell stage, 1- and 2-cell embryos were collected. When a P1 cell divided, a 3-minute timer was started, 9 and embryos were collected in pools. Each pool was timed for 10 minutes. After washing (taking ~2-3 mins) we checked that no 4-cell embryos were observed under the microscope prior to freezing. For each stage, this process was repeated until 9 embryos were collected in a single PCR tube.

Library Preparation

We used a slightly modified version of the previously described Ribo-ITP protocol [23]and a detailed protocol can be obtained from (https://ceniklab.github.io/ribo_itp/) which can be referred to for more details. In brief, the PCR tubes with 9 embryos were centrifuged to collect them at the bottom. We then added 2.5µl of 100µg/ml cycloheximide to the PCR tubes and we lysed the embryo by freeze thawing them in liquid nitrogen. We then added 2.5 µl of 2x lysis buffer (40mM Bistris, 100mM NaCl, 2% Triton-X-100, 10mM $MgCl_2$, 10 mM $CaCl_2$) and mixed well by pipetting. To obtain ribosome protected fragments, we added 1µl of 1:50 diluted MNase and incubated at 37°C for 30 mins. The digestion was then stopped using 1µl of 70mM EGTA and vortexed for at least 30 seconds and stored on ice. The microfluidics chip for ribosome profiling via isotachophoresis was setup and run as provided in [23]. The ribosome protected fragments were collected in dephosphorylation buffer from the Diagenode D-Plex Small RNA-seq Kit (Diagenode Cat. No C05030001) kit. The replicates for 1-cell (WT), 2-cell (WT), 4-cell (WT), 8-cell (WT), 1-cell (*zu405*), 2-cell (*zu405*) and 4-cell (*zu405*) were two, four, four, five, three, six, and four, respectively. We made a few modifications to the kit's library preparation protocol, and they were as follows. At the RNA-tailing step we used 0.5µl of Dephosphorylation Reagent along with 0.5µl of T4 Polynucleotide Kinase (New England Biolabs M0201L). Upon adding these two reagents the mixture is incubated for 25 mins at 37°C. Next, during

the reverse transcription with template switching, we diluted the TSO by half and used 2µl in the mixture. We used 16 cycles for the final PCR amplification to produce the DNA library. RNA libraries were prepared using the NEBNext® Single Cell/Low Input RNA Library Prep Kit for Illumina® (NEB #E6420S/L), following the manufacturer's protocol with some modifications. Briefly, embryo samples, each consisting of 9 embryos, were collected in PCR tubes containing 4.5 µl of water. These samples underwent a freeze-thaw cycle using liquid nitrogen to lyse the cells and release the RNA. For library preparation, we employed a two-step PCR amplification process. The initial cDNA enrichment PCR was performed for 14 cycles, followed by a final library amplification PCR for 8 cycles. Three independent biological replicates were prepared for each experimental condition.

Fixation and imaging of *C.elegans* embryos

To visualize CAM-1::mNG, LAG-1::mNG and DSH-2::mNG gravid hermaphrodites containing one row of embryos were selected alongside N2 controls. Twenty worms were dissected in 50 µL of 1X egg buffer (5 mM HEPES pH 7.4, 118 mM NaCl, 40 mM KCl, 3.4 mM $MgCl_2$, 3.4 mM $CaCl_2$) on a watch glass. One-cell embryos were collected within 2 minutes using 2.5 µL of 10% sodium hypochorite solution treatment and cleaned through sequential washes in Shelton's growth media (SGM; 0.5 mg/mL Inulin,5 mg/mL PVP, 1x BME vitamins, 1x Chemically Defined Lipid Concentrate and 1x Penicillin-Streptomycin added to Schneider's Drosophila Media) supplemented with 35% fetal bovine serum and then in 1X egg buffer. The following fixation protocol was modified from [85] . Embryos were fixed in pre-chilled (-20°C) methanol followed by two freeze-thaw cycles in liquid nitrogen. Samples were pelleted at 2000 × g in 30-second intervals with 180° rotation between spins for up to 5 minutes. After methanol removal, samples were incubated in -20°C acetone for 3 minutes, followed by centrifugation for up to 5 minutes. Fixed embryos underwent three 5-minute washes in 1X PBST, followed by incubation in 5% w/v BSA in PBST for 1 hour at 37°C with nutation. Samples were counterstained with DAPI (200 ng/µL) for 10 minutes and washed twice in PBST. Embryos were resuspended in 50 µL PBST and incubated at 4°C for 30 minutes. For imaging, 5 µL of sample was mounted between an L-polylysine-coated coverslip and glass slide, sealed with nail polish, and imaged using a Nikon Ti2 microscope controlled by µManager software and equipped with a 60x, 1.42 NA objective lens; a Visitich iSIM super-resolution confocal scan head; and a Photometrics Kinetix 22 camera. Imaging parameters included 405 nm and 505 nm channels with a 445-505-561-638 dichroic mirror. For live imaging, worms were dissected in egg buffer on L-polylysine-coated coverslips. Samples were sealed onto glass slides using valap and imaged immediately using identical conditions as the fixed samples.

13.3. Quantification AND Statistical analysis

Read alignment of ribosome profiling and RNA-seq data

Ribosome profiling data were processed using RiboFlow[77] Input data included gzipped fastq files containing ribosome profiling sequencing data, Bowtie2 index files for the transcriptome reference (appris_celegans_v1) and filter reference (rRNA sequences), a bed file defining CDS, UTR5, and UTR3 regions, and a two-column .tsv file containing transcript lengths. The reference files can be found here[44] : https://github.com/RiboBase/reference_caenorhabditis-elegans

Unique Molecular Identifiers (UMIs) were extracted from the reads using UMI-tools (Version 1.1.2) with the parameters "-p "^(?P<umi_1>.{12})(?P<discard_1>.{4}).+$" --extract-method=regex". Reads were processed using default settings[77] . Alignments with a mapping quality greater than two were retained. Deduplication was performed using UMI-tools[78] . Only footprints between 21 and 40 nucleotides in length were considered for the final analysis.

RiboFlow was also used to process the RNA-seq data. The processing steps were as follows: First, quality control and trimming were conducted using cutadapt (version 4.7), where the first and last 25 nucleotides were trimmed from each read with the parameters '-u 25 -u -25 --quality-cutoff=28'. Next, filtered reads were aligned using Bowtie2 in a two-step process: reads were initially aligned to a reference of rRNAs using the parameters '-L 15 --no-unal', and then unaligned reads were aligned to the transcriptome reference using the same parameters. Finally, in the post-alignment processing step, only alignments with a mapping quality greater than 2 were retained for further analysis.

Data Filtering and Processing

For each library, we first determined the footprint size range to be used in downstream analyses. Specifically, we selected the ones for which the percentage that mapped to CDS was greater than equal to 92.5 percent. Histone genes were excluded from the analysis due to their lack of poly-A tails, as our RNA-seq was generated using a oligo-dT based reverse transcription strategy (Table S1). A prior study has shown a systematic underestimation of histone transcript levels that prevents reliable calculation of their translational efficiency[86]. Histone genes were identified as the set of genes whose Wormbase Genetic gene nameID begins with “his”. We retained genes with a minimum of 3 counts per million in at least 10 of the 29 collected samples. Batch correction was then performed using ComBat-seq[81] by providing the day of library prep as the batch variable. These corrected counts were used for all subsequent analyses. We retained genes with a minimum of 10 counts per million in at least 18 of the 21 collected samples. Batch correction was then performed using ComBat-seq[81] by providing the day of library prep as variable to adjust for potential batch effects. These corrected counts were used for all subsequent analyses. Our final gene set consisted of 4,905 genes that passed both the ribosome profiling and RNA-seq filtering processes.

RNA abundance and Ribosome Occupancy correlation analysis

To analyze the relationship between ribosome occupancy and RNA abundance, we performed pairwise correlation analyses using normalized count data. Raw counts were first converted to counts per million (CPM) to account for differences in sequencing depth across samples. For both RNA-seq and Ribo-seq datasets, we calculated the mean CPM values across replicates for each gene. To assess data quality and reproducibility, we computed Spearman correlations between all possible pairs of replicates within each assay type (RNA-seq or Ribo-seq) and took their mean to obtain reliability scores. The observed correlation between mean ribosome occupancy and RNA abundance was then calculated using Spearman's rank correlation coefficient. To account for measurement noise in both assays, we applied a correction to the observed correlation using the reliability scores, calculated as:

$\rho_{corr} = \rho_{observed} / \sqrt{(rRNA \times rRibo)}$

Where rRNA and rRibo represent the reliability scores for RNA-seq and Ribo-seq measurements, respectively. Statistical analyses and visualizations were performed using R.

We analyzed datasets from two independent studies: Lee et al.(2020) and Quarato et al. (2021) to investigate the relationship between mRNA abundance and ribosome occupancy. First, we identified a set of common genes present in our and their datasets. For the Lee et al. (2020) dataset, we extracted average mRNA abundance (measured in Fragments Per Million, FPM) and average ribosome occupancy (also in FPM) for each gene. Similarly, for the Quarato et al. (2021) dataset, we extracted RNA abundance and ribosome occupancy values (measured in Transcripts Per Million, TPM).

Pairwise differential expression analysis

Differential expression analysis was performed using the edgeR package (version 4.0.16) in R. Library sizes were normalized using the trimmed mean of M-values method[87] . To identify differentially expressed genes between conditions, quasi-likelihood F-tests were performed using the glmQLFTest function. Contrasts were defined to specify the comparisons of interest, such as differences between consecutive developmental stages or between OMA-1/WT conditions in the case of comparing RNA abundance and ribosome occupancy. Translational efficiency changes were assessed using contrasts that compared the differences between Ribo-seq and RNA-seq data across different conditions or developmental stages

((Condition B Ribo-seq - Condition B RNA-seq) - (Condition A Ribo-seq - Condition A RNA-seq)).

This approach allowed for the identification of genes with significant changes in translational efficiency between the compared conditions, independent of changes in mRNA levels. For each comparison, genes with a false discovery rate (FDR) < 0.2 and $|\log_2 FC| > 1$ were considered significantly differentially expressed.

Normalization of TE

To get an estimate of TE at a given stage, we calculated the centered log-ratio (CLR) that account for the compositional nature of sequencing data[88] . The CLR of a gene is calculated as the natural logarithm of the ratio between x (defined as the count plus a pseudocount of 1) and the geometric mean of all genes in each replicate and sample.

$$clr(x) = \left[\ln \frac{x_1}{g(x)}; \ldots; \ln \frac{x_D}{g(x)}\right]$$

A pseudo count of +1 was added avoid zeros present in the ribosome profiling data. The resulting log-ratios were averaged across replicates. Translational efficiency (TE) was calculated as the difference between the averaged log-ratios of ribosome profiling and total RNA.

$$clr_{TE}(x) = clr_{ribo}(x) - clr_{RNA}(x)$$

This processed dataset, containing gene names and corresponding TE values, forms the basis for subsequent analyses of translational regulation during early embryonic development in *C. elegans*, both in wild-type and OMA-1 (*zu405*) conditions.

We compared our TE to two prior studies that obtained ribosome profiling data from *C.elegans* embryos[21,22] . For the Quarato et al. dataset[21], we used their reported centered log-ratio transformed translation efficiency values. For the Lee et al. dataset[22], we calculated log2 translation efficiency directly from their reported ribosome occupancy and mRNA abundance measurements. To assess the consistency of translation efficiency patterns across studies, we performed a comparative analysis between our stage-specific translation efficiency data and those from both published datasets. We focused on four early developmental stages: 1-cell, 2-cell, 4-cell, and 8-cell embryos. The spearman rank correlation was calculated between these two datasets.

Translational efficiency based on localization of transcripts

To categorize genes based on their spatial expression patterns, we utilized differential expression data from Tintori et al.[8] This dataset compared expression levels in whole embryos to those in germline precursor cells at two-cell, four-cell, and eight-cell stages. Genes were classified into three categories:

1. Somatic genes: $\log_2$ fold change > 1, adjusted p-value < 0.1, and $\log_2$ CPM > 4
2. Germline genes: $\log_2$ fold change < -1, adjusted p-value < 0.1, and $\log_2$ CPM > 4
3. Evenly expressed genes: |$\log_2$ fold change| < 1, adjusted p-value > 0.2, and $\log_2$ CPM > 4

The fold change values represent the expression ratio of (whole embryo)/(germline precursor cell). Thus, positive fold changes indicate higher expression in somatic cells, while negative fold changes suggest enrichment in germline precursors. Statistical differences in translational efficiency between somatic and germline-enriched transcripts were assessed using two-sided Wilcoxon rank-sum tests for each developmental stage. P-values < 0.05 were considered significant and visualized using asterisks (*p < 0.05, **p < 0.01, ***p < 0.001). Summary statistics including median, mean, standard deviation, and quartile values were calculated on R for each group at each developmental stage (see code) .

TE of P-granule localized transcripts

The localization of transcripts to P-granules was determined using single-molecule fluorescence in situ hybridization data from Scholl et al.[40] . For each transcript, P-granule association was assessed at the 2-cell (P1 cell), 4-cell (P2 cell), and 8-cell (P3 cell) stages. Differential translational efficiency between P-granule localized ("+") and non-localized ("-") transcripts was evaluated using two-sided Wilcoxon rank-sum tests at each developmental stage. For transcripts that transitioned into P-granules (from "-" to "+") between stages, changes in TE were assessed using paired Wilcoxon tests against a null hypothesis of no change. Additionally, differences in TE between Group I transcripts (maintained in P-granules through primordial germ cells) and Group II transcripts (transiently associated) were evaluated using Wilcoxon rank-sum tests at each stage. To assess the enrichment of P-granule transcripts in germline cells, Fisher's exact tests were performed comparing P-granule-localized transcripts with germline-enriched transcripts at each developmental stage. P-values < 0.05 were considered significant for all statistical tests.

Linear regression analysis of RNA-binding proteins

To investigate the relationship between 3' UTR motifs, RNA-binding protein interactions, and TE, we performed a series of analyses on data from one-cell, two-cell, four-cell, and eight-cell stage embryos. First, we converted the 3' UTR motif count data for POS-1,

MEX-3, and LIN-41 into binary format, where the presence of a motif was denoted as 1 and absence as 0. For OMA-1 and GLD-1, we used binary data from pull-down experiments to indicate protein-RNA interactions. We then merged this binary data with the log-normalized TE data based on gene names. A linear regression model was constructed to assess the influence of various factors on TE. For each developmental stage, we used the following predictors: OMA-1 pull-down status, presence of motifs for POS-1, MEX-3, and LIN-41, and GLD-1 pull-down status. The model for a given stage is represented as:

Translational Efficiency at stage X~ OMA_pulldown + POS1_motif + MEX3_motif + LIN41_motif + GLD_pulldown

We observed that 815 out of the 1039 transcripts pulled down with OMA-1 in oocytes[34] were detected robustly in our dataset. For each developmental stage (1-cell, 2-cell, 4-cell, and 8-cell), differences in translational efficiency (TE) between OMA-1-bound (n = 815) and unbound (n = 4090) transcripts were assessed using a two-sided Wilcoxon rank-sum test. The test statistic W is calculated as:

$$W = \sum(R_1) - [n_1(n_1 + 1)]/2$$

where R_1 is the sum of ranks for OMA-1-bound transcripts, n_1 is the number of bound transcripts, and the second term $[n_1(n_1 + 1)]/2$ represents the expected sum of ranks under the null hypothesis. The null hypothesis H_0 states that the TE distributions of bound and unbound transcripts are identical, while the alternative hypothesis H_1 states that the TE distributions differ between the two groups. This test was also applied for the violin plots generated for results in Figure S4.

Clustering analysis and GO enrichment

For wild-type (WT) data analysis, clustering was performed using k-means algorithm (k=9) on mean-centered data, where the mean expression value of each gene across all stages was subtracted. For visualization, the data was then normalized to the 1-cell stage by subtracting each gene's 1-cell stage value from all subsequent stages. For the comparative analysis between WT and OMA-1-depleted (OMA) conditions, data was first normalized to the 1-cell stage, then k-means clustering was performed with k=2 clusters for each condition independently on this 1-cell normalized data. The clustering results were combined to create multimodal clusters. Gene ontology (GO) enrichment analysis was conducted using the clusterProfiler package with the org.Ce.eg.db database for *C. elegans*. The background gene set for enrichment analysis was derived from all detected genes in the experiment. GO terms were simplified using the simplify() function with a cutoff of 0.5, and filtered based on enrichment ratio (>2) and adjusted p-value (<0.1). The complete GO enrichment results can be found in the supplement (Table S2 and S5). For

the main figure visualization, GO terms were manually curated to remove redundancy and highlight biologically relevant annotations.

14. References

1. Tadros, W., and Lipshitz, H.D. (2009). The maternal-to-zygotic transition: a play in two acts. Development *136*, 3033–3042. https://doi.org/10.1242/dev.033183.

2. Vastenhouw, N.L., Cao, W.X., and Lipshitz, H.D. (2019). The maternal-to-zygotic transition revisited. Development *146*, dev161471. https://doi.org/10.1242/dev.161471.

3. Winata, C.L., and Korzh, V. (2018). The translational regulation of maternal mRNAs in time and space. FEBS Lett. *592*, 3007–3023. https://doi.org/10.1002/1873-3468.13183.

4. COPELAND, P.R., and WORMINGTON, M. (2001). The mechanism and regulation of deadenylation: Identification and characterization of Xenopus PARN. RNA *7*, 875–886. https://doi.org/10.1017/s1355838201010020.

5. Simon, R., Tassan, J.P., and Richter, J.D. (1992). Translational control by poly(A) elongation during Xenopus development: differential repression and enhancement by a novel cytoplasmic polyadenylation element. Genes Dev. *6*, 2580–2591. https://doi.org/10.1101/gad.6.12b.2580.

6. Sulston, J.E., Schierenberg, E., White, J.G., and Thomson, J.N. (1983). The embryonic cell lineage of the nematode Caenorhabditis elegans. Dev Biol *100*, 64–119. https://doi.org/10.1016/0012-1606(83)90201-4.

7. Edgar, L.G., Wolf, N., and Wood, W.B. (1994). Early transcription in Caenorhabditis elegans embryos. Development *120*, 443–451. https://doi.org/10.1242/dev.120.2.443.

8. Tintori, S.C., Nishimura, E.O., Golden, P., Lieb, J.D., and Goldstein, B. (2016). A Transcriptional Lineage of the Early C. elegans Embryo. Dev Cell *38*, 430–444. https://doi.org/10.1016/j.devcel.2016.07.025.

9. Cenik, E.S., Meng, X., Tang, N.H., Hall, R.N., Arribere, J.A., Cenik, C., Jin, Y., and Fire, A. (2019). Maternal Ribosomes Are Sufficient for Tissue Diversification during Embryonic Development in C. elegans. Dev. Cell *48*, 811-826.e6. https://doi.org/10.1016/j.devcel.2019.01.019.

10. Nishimura, E.O., Zhang, J.C., Werts, A.D., Goldstein, B., and Lieb, J.D. (2015). Asymmetric Transcript Discovery by RNA-seq in C. elegans Blastomeres Identifies neg-1, a Gene Important for Anterior Morphogenesis. Plos Genet *11*, e1005117. https://doi.org/10.1371/journal.pgen.1005117.

11. Packer, J.S., Zhu, Q., Huynh, C., Sivaramakrishnan, P., Preston, E., Dueck, H., Stefanik, D., Tan, K., Trapnell, C., Kim, J., et al. (2019). A lineage-resolved molecular atlas of C. elegans embryogenesis at single-cell resolution. Science *365*. https://doi.org/10.1126/science.aax1971.

12. Hashimshony, T., Wagner, F., Sher, N., and Yanai, I. (2012). CEL-Seq: Single-Cell RNA-Seq by Multiplexed Linear Amplification. Cell Rep. *2*, 666–673. https://doi.org/10.1016/j.celrep.2012.08.003.

13. Jadhav, S., Rana, M., and Subramaniam, K. (2008). Multiple maternal proteins coordinate to restrict the translation of C. elegans nanos-2 to primordial germ cells. Development *135*, 1803–1812. https://doi.org/10.1242/dev.013656.

14. Farley, B.M., and Ryder, S.P. (2012). POS-1 and GLD-1 repress glp-1 translation through a conserved binding-site cluster. Mol. Biol. Cell *23*, 4473–4483. https://doi.org/10.1091/mbc.e12-03-0216.

15. Tabara, H., Hill, R.J., Mello, C.C., Priess, J.R., and Kohara, Y. (1999). pos-1 encodes a cytoplasmic zinc-finger protein essential for germline specification in C. elegans. Development *126*, 1–11. https://doi.org/10.1242/dev.126.1.1.

16. Elewa, A., Shirayama, M., Kaymak, E., Harrison, P.F., Powell, D.R., Du, Z., Chute, C.D., Woolf, H., Yi, D., Ishidate, T., et al. (2015). POS-1 Promotes Endo-mesoderm Development by Inhibiting the Cytoplasmic Polyadenylation of neg-1 mRNA. Dev. Cell *34*, 108–118. https://doi.org/10.1016/j.devcel.2015.05.024.

17. Gauvin, T.J., Han, B., Sun, M.J., and Griffin, E.E. (2018). PIE-1 Translation in the Germline Lineage Contributes to PIE-1 Asymmetry in the Early Caenorhabditis elegans Embryo. G3: GenesGenomesGenet. *8*, 3791–3801. https://doi.org/10.1534/g3.118.200744.

18. Oldenbroek, M., Robertson, S.M., Guven-Ozkan, T., Spike, C., Greenstein, D., and Lin, R. (2013). Regulation of maternal Wnt mRNA translation in C. elegans embryos. Development *140*, 4614–4623. https://doi.org/10.1242/dev.096313.

19. Winkenbach, L.P., Parker, D.M., Williams, R.T.P., and Nishimura, E.O. (2022). The ERM-1 membrane-binding domain directs erm-1 mRNA localization to the plasma membrane in the C. elegans embryo. Development. https://doi.org/10.1242/dev.200930.

20. Evans, T.C., Crittenden, S.L., Kodoyianni, V., and Kimble, J. (1994). Translational control of maternal glp-1 mRNA establishes an asymmetry in the C. elegans embryo. Cell *77*, 183–194. https://doi.org/10.1016/0092-8674(94)90311-5.

21. Quarato, P., Singh, M., Cornes, E., Li, B., Bourdon, L., Mueller, F., Didier, C., and Cecere, G. (2021). Germline inherited small RNAs facilitate the clearance of untranslated maternal mRNAs in C. elegans embryos. Nat Commun *12*, 1441. https://doi.org/10.1038/s41467-021-21691-6.

22. Lee, C.-Y.S., Putnam, A., Lu, T., He, S., Ouyang, J.P.T., and Seydoux, G. (2020). Recruitment of mRNAs to P granules by condensation with intrinsically-disordered proteins. eLife *9*, e52896. https://doi.org/10.7554/elife.52896.

23. Ozadam, H., Tonn, T., Han, C.M., Segura, A., Hoskins, I., Rao, S., Ghatpande, V., Tran, D., Catoe, D., Salit, M., et al. (2023). Single-cell quantification of ribosome occupancy in early mouse development. Nature *618*, 1057–1064. https://doi.org/10.1038/s41586-023-06228-9.

24. Han, C.M., Catoe, D., Munro, S.A., Khnouf, R., Snyder, M.P., Santiago, J.G., Salit, M.L., and Cenik, C. (2019). Simultaneous RNA purification and size selection using on-chip isotachophoresis with an ionic spacer. Lab a Chip *19*, 2741–2749. https://doi.org/10.1039/c9lc00311h.

25. Ingolia, N.T., Ghaemmaghami, S., Newman, J.R.S., and Weissman, J.S. (2009). Genome-Wide Analysis in Vivo of Translation with Nucleotide Resolution Using Ribosome Profiling. Science *324*, 218–223. https://doi.org/10.1126/science.1168978.

26. Ingolia, N.T., Lareau, L.F., and Weissman, J.S. (2011). Ribosome Profiling of Mouse Embryonic Stem Cells Reveals the Complexity and Dynamics of Mammalian Proteomes. Cell *147*, 789–802. https://doi.org/10.1016/j.cell.2011.10.002.

27. Albarqi, M.M.Y., and Ryder, S.P. (2023). The role of RNA-binding proteins in orchestrating germline development in Caenorhabditis elegans. Frontiers Cell Dev Biology *10*, 1094295. https://doi.org/10.3389/fcell.2022.1094295.

28. Draper, B.W., Mello, C.C., Bowerman, B., Hardin, J., and Priess, J.R. (1996). MEX-3 Is a KH Domain Protein That Regulates Blastomere Identity in Early C. elegans Embryos. Cell *87*, 205–216. https://doi.org/10.1016/s0092-8674(00)81339-2.

29. Schubert, C.M., Lin, R., Vries, C.J. de, Plasterk, R.H.A., and Priess, J.R. (2000). MEX-5 and MEX-6 Function to Establish Soma/Germline Asymmetry in Early C. elegans Embryos. Mol. Cell *5*, 671–682. https://doi.org/10.1016/s1097-2765(00)80246-4.

30. Gomes, J.-E., Encalada, S.E., Swan, K.A., Shelton, C.A., Carter, J.C., and Bowerman, B. (2001). The maternal gene spn-4 encodes a predicted RRM protein required for mitotic spindle orientation and cell fate patterning in early C. elegans embryos. Development *128*, 4301–4314. https://doi.org/10.1242/dev.128.21.4301.

31. Lin, R. (2003). A gain-of-function mutation in oma-1, a C. elegans gene required for oocyte maturation, results in delayed degradation of maternal proteins and embryonic lethality. Dev Biol *258*, 226–239. https://doi.org/10.1016/s0012-1606(03)00119-2.

32. Tsukamoto, T., Gearhart, M.D., Spike, C.A., Huelgas-Morales, G., Mews, M., Boag, P.R., Beilharz, T.H., and Greenstein, D. (2017). LIN-41 and OMA Ribonucleoprotein Complexes Mediate a Translational Repression-to-Activation Switch Controlling Oocyte Meiotic Maturation and the Oocyte-to-Embryo Transition in Caenorhabditis elegans. Genetics *206*, 2007–2039. https://doi.org/10.1534/genetics.117.203174.

33. Spike, C.A., Coetzee, D., Eichten, C., Wang, X., Hansen, D., and Greenstein, D. (2014). The TRIM-NHL Protein LIN-41 and the OMA RNA-Binding Proteins Antagonistically Control the

Prophase-to-Metaphase Transition and Growth of Caenorhabditis elegans Oocytes. Genetics *198*, 1535–1558. https://doi.org/10.1534/genetics.114.168831.

34. Spike, C.A., Coetzee, D., Nishi, Y., Guven-Ozkan, T., Oldenbroek, M., Yamamoto, I., Lin, R., and Greenstein, D. (2014). Translational Control of the Oogenic Program by Components of OMA Ribonucleoprotein Particles in Caenorhabditis elegans. Genetics *198*, 1513–1533. https://doi.org/10.1534/genetics.114.168823.

35. Kaymak, E., and Ryder, S.P. (2013). RNA Recognition by the Caenorhabditis elegans Oocyte Maturation Determinant OMA-1*. J Biol Chem *288*, 30463–30472. https://doi.org/10.1074/jbc.m113.496547.

36. Guven-Ozkan, T., Robertson, S.M., Nishi, Y., and Lin, R. (2010). zif-1 translational repression defines a second, mutually exclusive OMA function in germline transcriptional repression. Development *137*, 3373–3382. https://doi.org/10.1242/dev.055327.

37. Marinov, G.K., Williams, B.A., McCue, K., Schroth, G.P., Gertz, J., Myers, R.M., and Wold, B.J. (2014). From single-cell to cell-pool transcriptomes: Stochasticity in gene expression and RNA splicing. Genome Res. *24*, 496–510. https://doi.org/10.1101/gr.161034.113.

38. Hashimshony, T., Feder, M., Levin, M., Hall, B.K., and Yanai, I. (2015). Spatiotemporal transcriptomics reveals the evolutionary history of the endoderm germ layer. Nature *519*, 219–222. https://doi.org/10.1038/nature13996.

39. Seydoux, G., and Fire, A. (1994). Soma-germline asymmetry in the distributions of embryonic RNAs in Caenorhabditis elegans. Development *120*, 2823–2834. https://doi.org/10.1242/dev.120.10.2823.

40. Scholl, A., Liu, Y., and Seydoux, G. (2024). Caenorhabditis elegans germ granules accumulate hundreds of low translation mRNAs with no systematic preference for germ cell fate regulators. Dev. (Camb., Engl.) *151*, dev202575. https://doi.org/10.1242/dev.202575.

41. Brar, G.A., and Weissman, J.S. (2015). Ribosome profiling reveals the what, when, where and how of protein synthesis. Nat. Rev. Mol. Cell Biol. *16*, 651–664. https://doi.org/10.1038/nrm4069.

42. Yadav, V., Irshad, I.U., Kumar, H., and Sharma, A.K. (2021). Quantitative Modeling of Protein Synthesis Using Ribosome Profiling Data. Front. Mol. Biosci. *8*, 688700. https://doi.org/10.3389/fmolb.2021.688700.

43. Andreev, D.E., O'Connor, P.B.F., Loughran, G., Dmitriev, S.E., Baranov, P.V., and Shatsky, I.N. (2017). Insights into the mechanisms of eukaryotic translation gained with ribosome profiling. Nucleic Acids Res. *45*, 513–526. https://doi.org/10.1093/nar/gkw1190.

44. Liu, Y., Hoskins, I., Geng, M., Zhao, Q., Chacko, J., Qi, K., Persyn, L., Wang, J., Zheng, D., Zhong, Y., et al. (2024). Translation efficiency covariation across cell types is a conserved

organizing principle of mammalian transcriptomes. bioRxiv, 2024.08.11.607360. https://doi.org/10.1101/2024.08.11.607360.

45. Liu, T.-Y., Huang, H.H., Wheeler, D., Xu, Y., Wells, J.A., Song, Y.S., and Wiita, A.P. (2017). Time-Resolved Proteomics Extends Ribosome Profiling-Based Measurements of Protein Synthesis Dynamics. Cell Syst. *4*, 636-644.e9. https://doi.org/10.1016/j.cels.2017.05.001.

46. Rubio, A., Ghosh, S., Mülleder, M., Ralser, M., and Mata, J. (2020). Ribosome profiling reveals ribosome stalling on tryptophan codons and ribosome queuing upon oxidative stress in fission yeast. Nucleic Acids Res. *49*, 383–399. https://doi.org/10.1093/nar/gkaa1180.

47. Chyżyńska, K., Labun, K., Jones, C., Grellscheid, S.N., and Valen, E. (2021). Deep conservation of ribosome stall sites across RNA processing genes. NAR Genom. Bioinform. *3*, lqab038. https://doi.org/10.1093/nargab/lqab038.

48. Quinn, T.P., Erb, I., Richardson, M.F., and Crowley, T.M. (2018). Understanding sequencing data as compositions: an outlook and review. Bioinformatics *34*, 2870–2878. https://doi.org/10.1093/bioinformatics/bty175.

49. Stoeckius, M., Grün, D., Kirchner, M., Ayoub, S., Torti, F., Piano, F., Herzog, M., Selbach, M., and Rajewsky, N. (2014). Global characterization of the oocyte-to-embryo transition in Caenorhabditis elegans uncovers a novel mRNA clearance mechanism. Embo J *33*, 1751–1766. https://doi.org/10.15252/embj.201488769.

50. Peng, F., Nordgren, C.E., and Murray, J.I. (2024). A spatiotemporally resolved atlas of mRNA decay in the C. elegans embryo reveals differential regulation of mRNA stability across stages and cell types. bioRxiv, 2024.01.15.575757. https://doi.org/10.1101/2024.01.15.575757.

51. Huang, N.N., and Hunter, C.P. (2015). The RNA binding protein MEX-3 retains asymmetric activity in the early Caenorhabditis elegans embryo in the absence of asymmetric protein localization. Gene *554*, 160–173. https://doi.org/10.1016/j.gene.2014.10.042.

52. Hunter, C.P., and Kenyon, C. (1996). Spatial and Temporal Controls Target pal-1 Blastomere-Specification Activity to a Single Blastomere Lineage in C. elegans Embryos. Cell *87*, 217–226. https://doi.org/10.1016/s0092-8674(00)81340-9.

53. Bowerman, B., Draper, B.W., Mello, C.C., and Priess, J.R. (1993). The maternal gene skn-1 encodes a protein that is distributed unequally in early C. elegans embryos. Cell *74*, 443–452. https://doi.org/10.1016/0092-8674(93)80046-h.

54. Baugh, L.R., Hill, A.A., Claggett, J.M., Hill-Harfe, K., Wen, J.C., Slonim, D.K., Brown, E.L., and Hunter, C.P. (2005). The homeodomain protein PAL-1 specifies a lineage-specific regulatory network in the C. elegans embryo. Development *132*, 1843–1854. https://doi.org/10.1242/dev.01782.

55. D'Agostino, I., Merritt, C., Chen, P.-L., Seydoux, G., and Subramaniam, K. (2006). Translational repression restricts expression of the C. elegans Nanos homolog NOS-2 to the embryonic germline. Dev. Biol. *292*, 244–252. https://doi.org/10.1016/j.ydbio.2005.11.046.

56. Heppert, J.K., Pani, A.M., Roberts, A.M., Dickinson, D.J., and Goldstein, B. (2018). A CRISPR Tagging-Based Screen Reveals Localized Players in Wnt-Directed Asymmetric Cell Division. Genetics *208*, 1147–1164. https://doi.org/10.1534/genetics.117.300487.

57. Parker, D.M., Winkenbach, L.P., Boyson, S., Saxton, M.N., Daidone, C., Al-Mazaydeh, Z.A., Nishimura, M.T., Mueller, F., and Nishimura, E.O. (2020). mRNA localization is linked to translation regulation in the Caenorhabditis elegans germ lineage. Development *147*, dev186817. https://doi.org/10.1242/dev.186817.

58. Baugh, L.R., Hill, A.A., Slonim, D.K., Brown, E.L., and Hunter, C.P. (2003). Composition and dynamics of the Caenorhabditis elegans early embryonic transcriptome. Development *130*, 889–900. https://doi.org/10.1242/dev.00302.

59. Oldenbroek, M., Robertson, S.M., Guven-Ozkan, T., Gore, S., Nishi, Y., and Lin, R. (2012). Multiple RNA-binding proteins function combinatorially to control the soma-restricted expression pattern of the E3 ligase subunit ZIF-1. Dev Biol *363*, 388–398. https://doi.org/10.1016/j.ydbio.2012.01.002.

60. Wright, J.E., Gaidatzis, D., Senften, M., Farley, B.M., Westhof, E., Ryder, S.P., and Ciosk, R. (2011). A quantitative RNA code for mRNA target selection by the germline fate determinant GLD-1. EMBO J. *30*, 533–545. https://doi.org/10.1038/emboj.2010.334.

61. Farley, B.M., Pagano, J.M., and Ryder, S.P. (2008). RNA target specificity of the embryonic cell fate determinant POS-1. RNA *14*, 2685–2697. https://doi.org/10.1261/rna.1256708.

62. Pagano, J.M., Farley, B.M., Essien, K.I., and Ryder, S.P. (2009). RNA recognition by the embryonic cell fate determinant and germline totipotency factor MEX-3. Proc National Acad Sci *106*, 20252–20257. https://doi.org/10.1073/pnas.0907916106.

63. Detwiler, M.R., Reuben, M., Li, X., Rogers, E., and Lin, R. (2001). Two Zinc Finger Proteins, OMA-1 and OMA-2, Are Redundantly Required for Oocyte Maturation in C. elegans. Dev Cell *1*, 187–199. https://doi.org/10.1016/s1534-5807(01)00026-0.

64. Dunn, J.G., Foo, C.K., Belletier, N.G., Gavis, E.R., and Weissman, J.S. (2013). Ribosome profiling reveals pervasive and regulated stop codon readthrough in Drosophila melanogaster. eLife *2*, e01179. https://doi.org/10.7554/elife.01179.

65. Singleman, C., and Holtzman, N.G. (2014). Growth and Maturation in the Zebrafish, Danio Rerio: A Staging Tool for Teaching and Research. Zebrafish *11*, 396–406. https://doi.org/10.1089/zeb.2014.0976.

66. Zahn, N., James-Zorn, C., Ponferrada, V.G., Adams, D.S., Grzymkowski, J., Buchholz, D.R., Nascone-Yoder, N.M., Horb, M., Moody, S.A., Vize, P.D., et al. (2022). Normal Table of Xenopus development: a new graphical resource. Development *149*, dev200356. https://doi.org/10.1242/dev.200356.

67. Edgar, B.A., and Schubiger, G. (1986). Parameters controlling transcriptional activation during early drosophila development. Cell *44*, 871–877. https://doi.org/10.1016/0092-8674(86)90009-7.

68. Shermoen, A.W., and O'Farrell, P.H. (1991). Progression of the cell cycle through mitosis leads to abortion of nascent transcripts. Cell *67*, 303–310. https://doi.org/10.1016/0092-8674(91)90182-x.

69. O'Farrell, P.H., Stumpff, J., and Su, T.T. (2004). Embryonic Cleavage Cycles: How Is a Mouse Like a Fly? Curr. Biol. *14*, R35–R45. https://doi.org/10.1016/j.cub.2003.12.022.

70. Wang, J., Garrey, J., and Davis, R.E. (2014). Transcription in Pronuclei and One- to Four-Cell Embryos Drives Early Development in a Nematode. Curr. Biol. *24*, 124–133. https://doi.org/10.1016/j.cub.2013.11.045.

71. Spirov, A., Fahmy, K., Schneider, M., Frei, E., Noll, M., and Baumgartner, S. (2009). Formation of the bicoid morphogen gradient: an mRNA gradient dictates the protein gradient. Development *136*, 605–614. https://doi.org/10.1242/dev.031195.

72. Medioni, C., Mowry, K., and Besse, F. (2012). Principles and roles of mRNA localization in animal development. Development *139*, 3263–3276. https://doi.org/10.1242/dev.078626.

73. Hawdon, A., Geoghegan, N.D., Mohenska, M., Elsenhans, A., Ferguson, C., Polo, J.M., Parton, R.G., and Zenker, J. (2023). Apicobasal RNA asymmetries regulate cell fate in the early mouse embryo. Nat. Commun. *14*, 2909. https://doi.org/10.1038/s41467-023-38436-2.

74. Thomas, L., Putnam, A., and Folkmann, A. (2023). Germ granules in development. Development *150*, dev201037. https://doi.org/10.1242/dev.201037.

75. Dufourt, J., Bellec, M., Trullo, A., Dejean, M., Rossi, S.D., Favard, C., and Lagha, M. (2021). Imaging translation dynamics in live embryos reveals spatial heterogeneities. Science *372*, 840–844. https://doi.org/10.1126/science.abc3483.

76. Salm, E. van der, Koelewijn, E., Maas, E. van der, Eeken, M., and Ruijtenberg, S. (2024). Localized translation of erm-1 contributes to ERM-1 function in the C. elegans embryo. bioRxiv, 2024.09.23.614538. https://doi.org/10.1101/2024.09.23.614538.

77. Ozadam, H., Geng, M., and Cenik, C. (2020). RiboFlow, RiboR and RiboPy: an ecosystem for analyzing ribosome profiling data at read length resolution. Bioinformatics *36*, 2929–2931. https://doi.org/10.1093/bioinformatics/btaa028.

78. Smith, T., Heger, A., and Sudbery, I. (2017). UMI-tools: modeling sequencing errors in Unique Molecular Identifiers to improve quantification accuracy. Genome Res. *27*, 491–499. https://doi.org/10.1101/gr.209601.116.

79. Langmead, B., and Salzberg, S.L. (2012). Fast gapped-read alignment with Bowtie 2. Nat. Methods *9*, 357–359. https://doi.org/10.1038/nmeth.1923.

80. Martin, M. (2011). Cutadapt removes adapter sequences from high-throughput sequencing reads. EMBnet.journal *17*, 10–12. https://doi.org/10.14806/ej.17.1.200.

81. Zhang, Y., Parmigiani, G., and Johnson, W.E. (2020). ComBat-seq: batch effect adjustment for RNA-seq count data. NAR Genom. Bioinform. *2*, lqaa078. https://doi.org/10.1093/nargab/lqaa078.

82. Robinson, M.D., McCarthy, D.J., and Smyth, G.K. (2010). edgeR: a Bioconductor package for differential expression analysis of digital gene expression data. Bioinformatics *26*, 139–140. https://doi.org/10.1093/bioinformatics/btp616.

83. Yu, G., Wang, L.-G., Han, Y., and He, Q.-Y. (2012). clusterProfiler: an R Package for Comparing Biological Themes Among Gene Clusters. OMICS: A J. Integr. Biol. *16*, 284–287. https://doi.org/10.1089/omi.2011.0118.

84. Edelstein, A.D., Tsuchida, M.A., Amodaj, N., Pinkard, H., Vale, R.D., and Stuurman, N. (2014). Advanced methods of microscope control using μManager software. J. Biol. Methods *1*, 1. https://doi.org/10.14440/jbm.2014.36.

85. Parker, D.M., Winkenbach, L.P., Parker, A., Boyson, S., and Nishimura, E.O. (2021). Improved Methods for Single-Molecule Fluorescence In Situ Hybridization and Immunofluorescence in Caenorhabditis elegans Embryos. Curr. Protoc. *1*, e299. https://doi.org/10.1002/cpz1.299.

86. Cenik, C., Cenik, E.S., Byeon, G.W., Grubert, F., Candille, S.I., Spacek, D., Alsallakh, B., Tilgner, H., Araya, C.L., Tang, H., et al. (2015). Integrative analysis of RNA, translation, and protein levels reveals distinct regulatory variation across humans. Genome Res. *25*, 1610–1621. https://doi.org/10.1101/gr.193342.115.

87. Robinson, M.D., and Oshlack, A. (2010). A scaling normalization method for differential expression analysis of RNA-seq data. Genome Biol. *11*, R25. https://doi.org/10.1186/gb-2010-11-3-r25.

88. Quinn, T.P., Richardson, M.F., Lovell, D., and Crowley, T.M. (2017). propr: An R-package for Identifying Proportionally Abundant Features Using Compositional Data Analysis. Sci. Rep. *7*, 16252. https://doi.org/10.1038/s41598-017-16520-0.